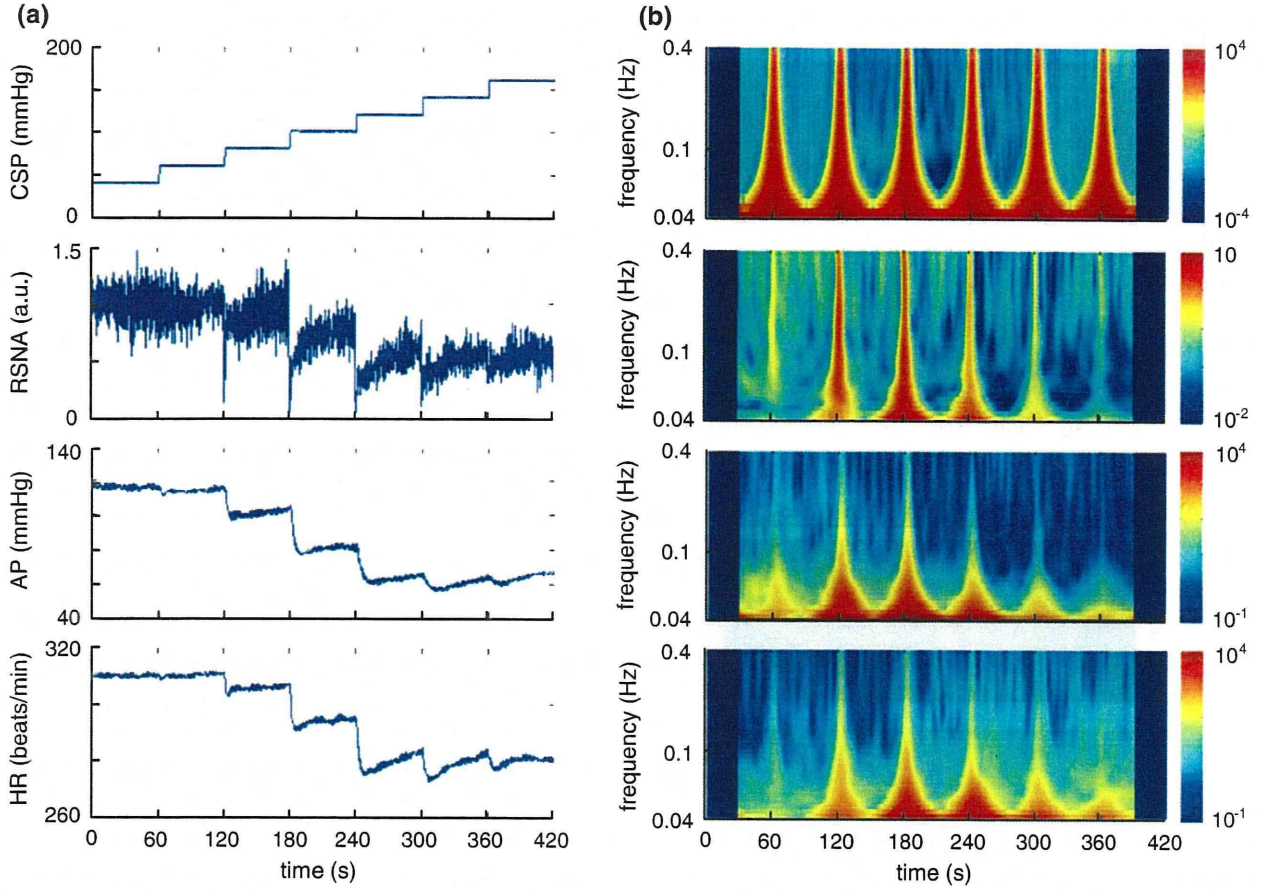

FIGURE 3. Averaged time series (a, $n = 8$) and wavelet power (b, $n = 8$) of CSP, renal sympathetic nerve activities (RSNA), AP, and heart rate (HR) during the static protocol. CSP was increased from 40 to 160 mmHg in 20 mmHg increments, resulting in changes of RSNA, AP, and HR through the carotid sinus baroreflex.

CSP_{40-60} and $CSP_{140-160}$ changes than other CSP changes.

Figure 5 and Table 1 show the average gain and phase ($n = 8$) in the neural arc (a), peripheral arc (b), total loop (c), and cardiac baroreflex (d). In the neural arc, $G_{0.04}$ (2.42 ± 0.07 a.u./mmHg) at the CSP_{80-100} change was the highest among all CSP changes, and was almost four to five times higher than those at the CSP_{40-60} (0.54 ± 0.09, $p < 0.01$) and $CSP_{140-160}$ (0.62 ± 0.06, $p < 0.01$) changes. Slopes increased significantly at lower and higher CSP changes compared with the $CSP_{100-120}$ change. Lag time at CSP_{80-100} was the shortest among all CSP changes. In the peripheral arc, Slope and lag time did not differ significantly among the CSP changes, whereas $G_{0.04}$ showed a tendency to decrease slightly with increase of CSP. In the total baroreflex, $G_{0.04}$ at CSP_{80-100} change (1.28 ± 0.12) was significantly higher compared to other CSP changes. Slopes were significantly greater at CSP changes within 60–120 mmHg than other CSP changes. Lag time did not differ significantly among CSP changes. In the cardiac baroreflex, $G_{0.04}$ (0.90 ± 0.18 and 0.92 ± 0.19 beats/min/mmHg) and Slopes were significantly higher at CSP_{80-100} and $CSP_{100-120}$ changes than other CSP changes. There were no significant differences in lag time among CSP changes.

Static Baroreflex

The static characteristics of the total loop were averaged ($n = 8$). Regression analysis was performed for logistic functions. Response range, coefficient of gain, midpoint of input axis, and minimum value of output were 0.45, 0.11, 99.6, and 0.55 in the neural arc, 65.2, 0.07, 97.6, and 69.4 in the total loop, and 29.5, 0.11, 98.2, and 281.2 in the cardiac baroreflex. Linear regression analysis was performed in the peripheral arc (static gain = 0.0086 and offset pressure = 0.027). The intersection between the CSP-AP curve and the line of identity corresponds to AP_{OP} (94.3 mmHg) located in the steepest portion (80–100 mmHg) of the sigmoid

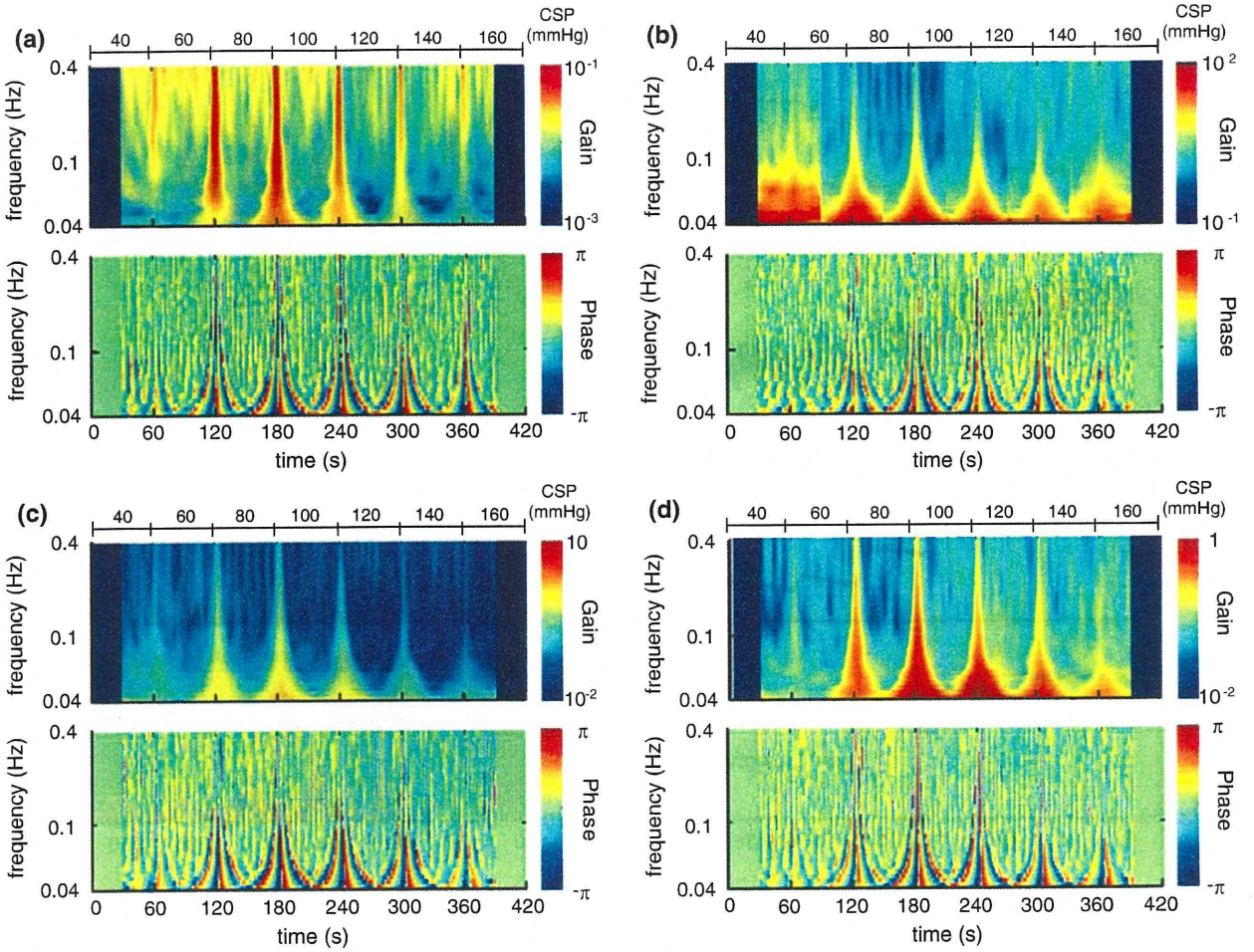

FIGURE 4. Time course of transfer functions of the neural arc from CSP to RSNA (a), peripheral arc from RSNA to AP (b), total baroreflex loop from CSP to AP (c), and cardiac baroreflex from CSP to HR (d) averaged across all animals (n = 8).

curve. In the equilibrium diagram, RSNA decreased with increasing CSP in the neural arc, AP increased with increasing RSNA in the peripheral arc, and the intersection between the two arcs provided the AP_{OP} (99.7 mmHg). In the cardiac baroreflex, HR decreased with the increase in CSP.

Bezold-Jarisch Reflex

In the total loop and cardiac baroreflex, the gains at various CSP changes during the BJR were identified ($n = 8$, Fig. 6 and Table 2). Averages of gain and phase (Fig. 6d) were derived from the time series in Figs. 6b and 6c. At middle CSP change of the total loop, $G_{0.04}$ was approximately halved under PBG condition compared to Control (0.59 ± 0.09 vs. 1.39 ± 0.15, $p < 0.01$). Slope and lag time did not differ significantly between the PBG and Control conditions at all CSP changes. In the cardiac baroreflex (Fig. 6e), $G_{0.04}$ tended to modulate under PBG condition at low and high CSP changes, but did not differ significantly between the two conditions at middle CSP changes. Slope differed significantly between the two conditions at low CSP change whereas lag time did not differ significantly at all CSP changes.

Cardiac Baroreflex

The ratio of the cardiac baroreflex to the total loop in dynamic characteristics was studied (Fig. 7). For CSP changes within 60–120 mmHg under Control condition, the ratios were almost linear and increased slightly with increase in frequency; in lower or higher CSP changes, they were modulated especially around 0.2 Hz. For CSP changes under PBG condition, overall the ratios were higher than those under Control condition. For CSP changes within 80–120 mmHg under PBG condition, the ratios were almost linear and the slopes were greater than those of Control condition; in lower or higher CSP changes, they

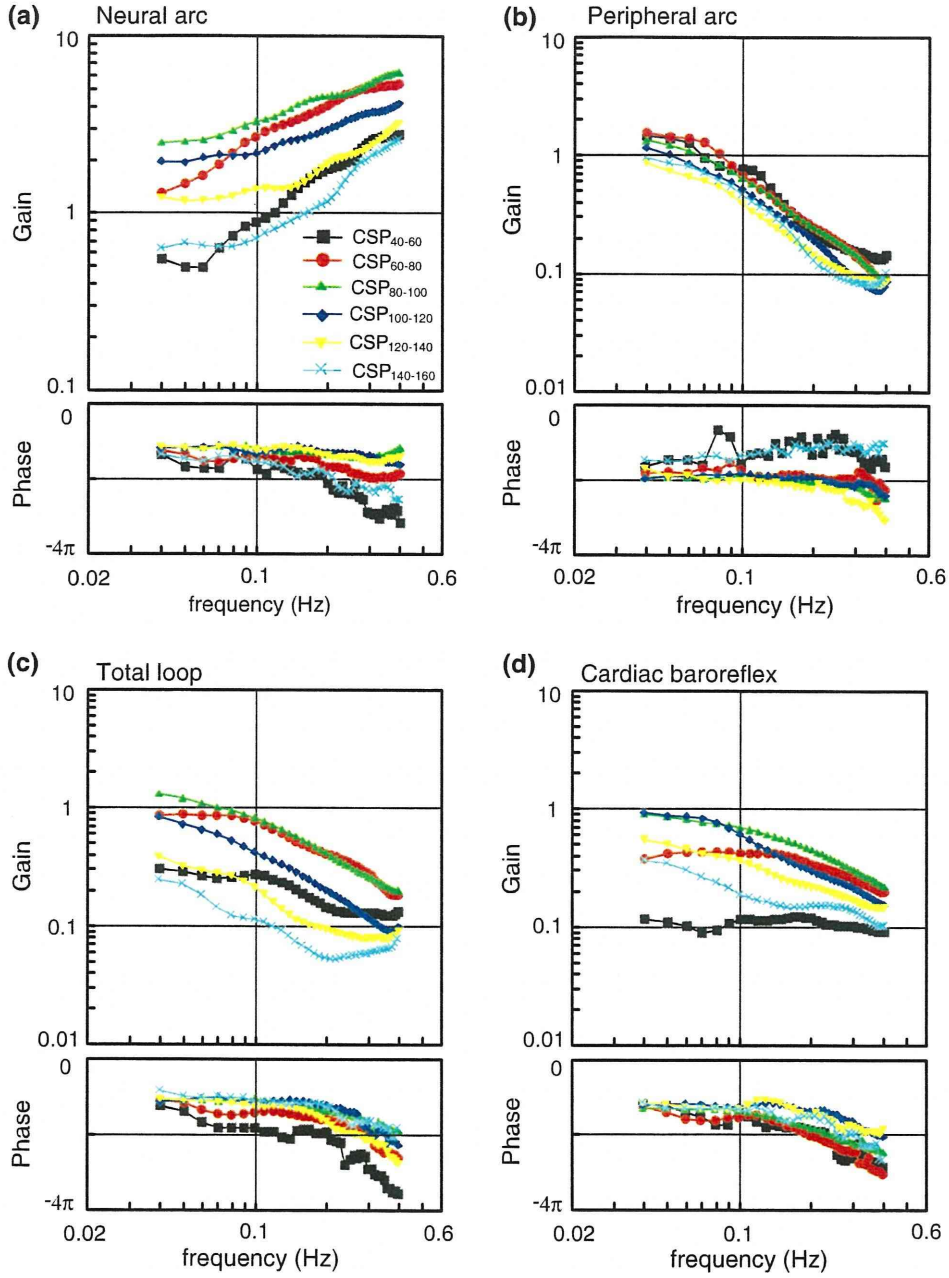

FIGURE 5. Transfer functions of the neural arc from CSP to RSNA, effective peripheral arc from RSNA to AP, total baroreflex loop from CSP to AP, and cardiac baroreflex estimated by wavelet analysis. Average (n = 8) gain (*top*) and phase (*bottom*).

increased within the 0.1–0.2 Hz range and decreased at higher frequencies. The phase difference did not differ among CSP changes under both Control and PBG conditions.

Closed-Loop Baroreflex

Simulation was performed using a cardiac baroreflex system from closed-loop AP input to HR output (Fig. 8a). To test the proposed wavelet analysis, an external disturbance to AP (AP_{noise} = +20 mmHg) was added to the system, and HR responses under carotid sinus open- and closed-loop AP responses were calculated (Fig. 8b). The observed AP and HR (AP_{change} and HR_{change}) were modulated by closed-loop regulation of AP. The CSP is identical with the observed AP_{change}. Gain and phase in the time series (Fig. 8c) and extracted (Fig. 8d) transfer functions were accurately estimated under open and closed AP responses.

TABLE 1. Parameters of the transfer functions in the neural arc, peripheral arc, total loop, and cardiac baroreflex at various step pressure inputs.

	CSP (mmHg)					
	40–60	60–80	80–100	100–120	120–140	140–160
Neural arc						
$G_{0.04}$ (a.u./mmHg)	0.54 ± 0.09	1.25 ± 0.17**	2.42 ± 0.07**,††	1.89 ± 0.13**,†	1.18 ± 0.20*,‡‡,¶¶	0.62 ± 0.06†,‡‡,¶¶
Slope (dB/decade)	17.9 ± 4.1	10.0 ± 1.9	7.7 ± 2.0	5.8 ± 3.1*	11.0 ± 1.8	16.8 ± 3.1¶
Lag time (s)	2.63 ± 0.58	0.78 ± 0.16*	0.27 ± 0.18**	0.48 ± 0.14**	0.45 ± 0.17**	1.83 ± 0.71
Peripheral arc						
$G_{0.04}$ (mmHg/a.u.)	1.42 ± 0.17	1.50 ± 0.18	1.30 ± 0.08	1.13 ± 0.13	0.85 ± 0.10†	0.92 ± 0.09†
Slope (dB/decade)	−24.6 ± 3.3	−29.4 ± 1.3	−28.2 ± 0.8	−26.6 ± 2.8	−22.7 ± 2.8	−23.2 ± 4.6
Lag time (s)	0.40 ± 0.79	1.29 ± 0.20	1.35 ± 0.20	1.35 ± 0.58	2.10 ± 0.69	0.08 ± 0.64
Total loop						
$G_{0.04}$	0.29 ± 0.05	0.85 ± 0.16**	1.28 ± 0.12**,††	0.83 ± 0.09**,‡‡	0.38 ± 0.07††,‡‡,¶¶	0.24 ± 0.04††,‡‡,¶¶
Slope (dB/decade)	−6.8 ± 4.1	−19.4 ± 2.4**	−20.5 ± 1.6**	−20.7 ± 2.1**	−11.8 ± 2.7	−6.4 ± 4.1††,‡‡,¶¶
Lag time (s)	3.03 ± 0.61	2.07 ± 0.12	1.62 ± 0.20	1.82 ± 0.60	2.54 ± 0.62	1.91 ± 0.41
Cardiac baroreflex						
$G_{0.04}$ (beats/min/mmHg)	0.11 ± 0.02	0.37 ± 0.11	0.90 ± 0.18**,††	0.92 ± 0.19**,††	0.55 ± 0.12**,‡,¶	0.36 ± 0.09‡‡,¶¶
Slope (dB/decade)	−2.3 ± 2.1	−10.7 ± 2.3	−15.9 ± 2.8**	−19.0 ± 2.9**	−11.8 ± 2.6	−6.3 ± 3.1‡,¶¶
Lag time (s)	2.13 ± 0.62	2.26 ± 0.34	2.17 ± 0.62	1.51 ± 0.16	1.70 ± 0.61	1.92 ± 0.86

$G_{0.04}$, transfer gain at 0.04 Hz. Slope, average slope of transfer gain between 0.1 and 0.4 Hz.
$p < 0.01$; ** vs. 40–60, †† vs. 60–80, ‡‡ vs. 80–100, and ¶¶ vs. 100–120 mmHg in CSP change; the same symbols of a single show $p < 0.05$.

DISCUSSION

We have shown that the analysis using wavelet transform can identify the dynamic baroreflex properties at various pressure levels from the time-course data under normal (Fig. 5) and pathophysiological conditions (Fig. 6) with background noise. The results of the proposed analysis applied in animal experiments indicate the possibility of its use in the assessment of human baroreflex (Figs. 7 and 8).

Time-Series Analysis for Dynamic Baroreflex

Under the background noise added to the response model, the proposed analysis applied to step response was able to detect the dynamic baroreflex characteristics (Fig. 2). The standard spectral analysis under stationary conditions has high reliability in the baroreflex test, and uses longer data to cancel the noise[31,38] at various pressure inputs and lose the short-term and important changes. In direct calculation of the dynamic characteristics from the step input output data, the traditional time series analysis might also have a disadvantage under noise contamination, which may cause poor S/N ratio in the impaired baroreflex function of cardiac diseases.[41] The STFFT using time windows of a constant range for all frequencies was actually unable to catch the dynamic property especially at higher frequencies under such condition (Figs. 1 and 2d) because of the average one within the whole time window. On the other hand, the modified wavelet-based analysis with improved temporal resolution at higher frequencies to reasonably catch the localized changes in cardiovascular control[4,50] will be effective for extracting the dynamic baroreflex characteristics under nonstationary hemodynamics with a low S/N ratio. Because the baroreflex test may depend on the various S/N ratios depending on the system input (e.g. amplitude) and/or the background noises, further investigations will be required in this regard.

Burgess *et al.*[2] showed that cross spectrum analysis using wavelet transform characterized strong coupling between sympathetic nerve traffic and AP at frequencies of <0.1 Hz. Davrath *et al.*[4] reported that time-varying power obtained from wavelet transform of the spontaneous HR or AP fluctuation in humans are remarkably modulated at approximately 0.1 Hz under standing condition. Whereas the traditional wavelet analysis could extract the localized characteristics of time-series data in a nonstationary condition,[2,4] application to dynamic system identification is difficult because of the limitation in phase extraction. When the same time window is set for the input and output data, the actual information of phase and gain may be lost or split, instead of high temporal resolution of wavelet transform.[34] To apply wavelet analysis to the baroreflex system identification, we expanded the basic analysis by acquiring the transfer function from maximum input and output data. The proposed method was able to acquire the system identification of baroreflex because of the specific characteristics of wavelet

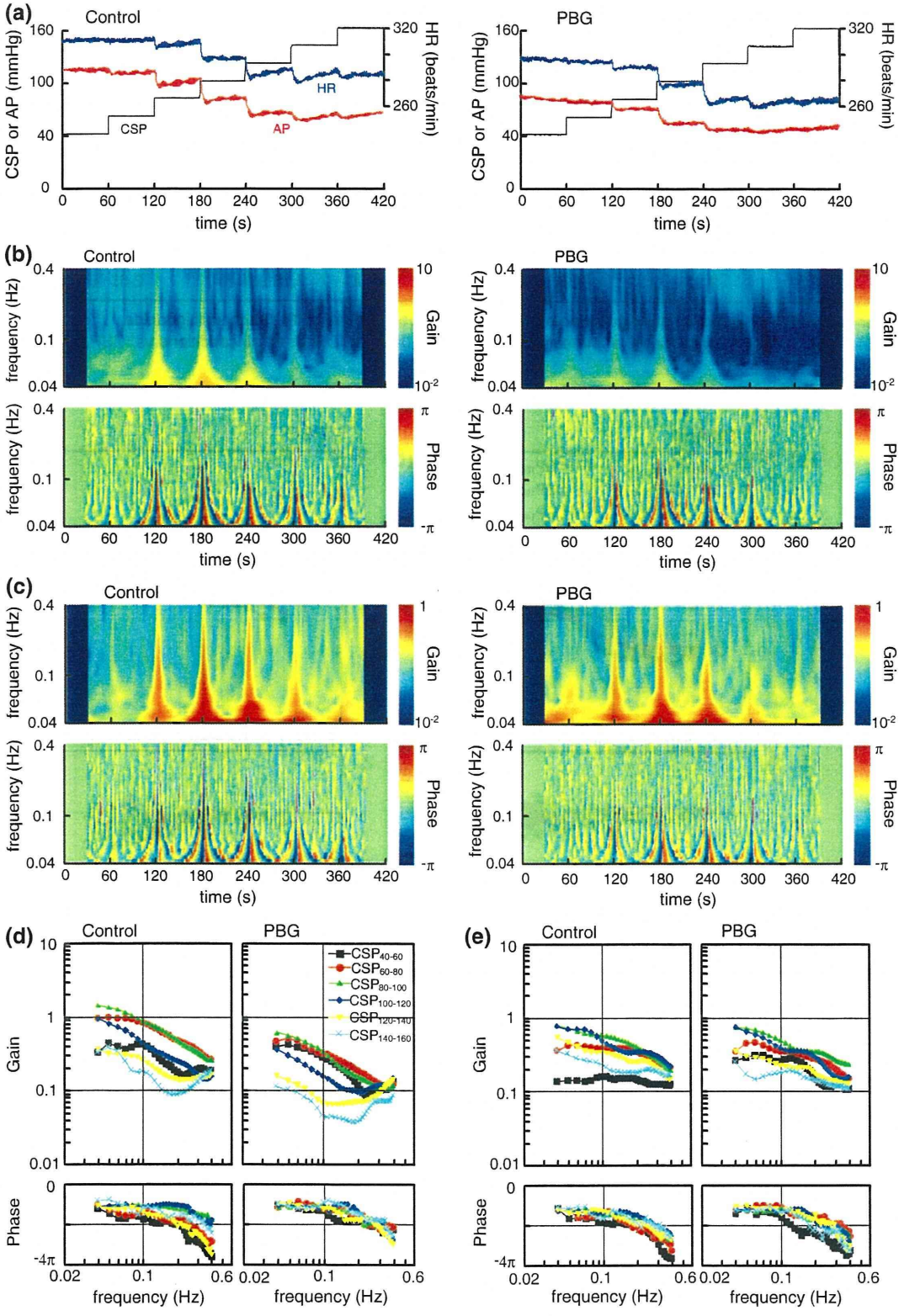

FIGURE 6. (a) Averaged (n = 8) time series of CSP, AP, and HR obtained in the absence (Control, *left*) and presence of phenylbiguanide (PBG, *right*). CSP was increased from 40 to 160 mmHg in 20 mmHg increments, resulting in changes in AP and HR through the carotid sinus baroreflex. Time-series transfer functions of total loop (b) and cardiac baroreflex (c) in the Control (*left*) and PBG (*right*) conditions. Average (n = 8) gain (*top*) and phase (*bottom*). Transfer functions of total loop (d) and cardiac baroreflex (e) estimated by wavelet analysis in the Control (*left*) and PBG (*right*) conditions.

TABLE 2. Parameters of the transfer functions for the total loop and cardiac baroreflex before and during PBG infusion.

	Low CSP (40–60 mmHg)		Middle CSP (80–100 mmHg)		High CSP (120–140 mmHg)	
	Control	PBG	Control	PBG	Control	PBG
Total loop						
$G_{0.04}$	0.32 ± 0.07	0.39 ± 0.09††	1.39 ± 0.15	0.59 ± 0.09**,††	0.35 ± 0.04††	0.15 ± 0.02††
Slope (dB/decade)	−11.6 ± 3.3	−8.0 ± 4.2	−17.8 ± 2.1	−15.0 ± 3.2	−6.5 ± 2.5	7.4 ± 5.3††
Lag time (s)	2.90 ± 0.71	1.43 ± 0.68	1.44 ± 0.22	2.21 ± 0.59	3.48 ± 0.61	2.74 ± 0.89
Cardiac baroreflex						
$G_{0.04}$ (beats/min/mmHg)	0.14 ± 0.02	0.26 ± 0.10†	0.78 ± 0.21	0.75 ± 0.18	0.54 ± 0.13	0.35 ± 0.08†
Slope (dB/decade)	−1.8 ± 2.2	−12.5 ± 2.9*	−13.4 ± 2.7	−11.6 ± 2.1	−12.6 ± 2.7	−6.6 ± 4.0
Lag time (s)	2.99 ± 0.89	2.91 ± 0.55	2.06 ± 0.30	2.28 ± 0.54	2.65 ± 0.72	2.47 ± 0.77

$G_{0.04}$, transfer gain at 0.04 Hz. Slope, average slope of gain between 0.1 and 0.4 Hz. PBG, phenylbiguanide.
** $p < 0.01$ and * $p < 0.05$, PBG vs. Control at the same CSP; †† $p < 0.01$ and † $p < 0.05$, all conditions vs. CSP_{80-100} of Control.

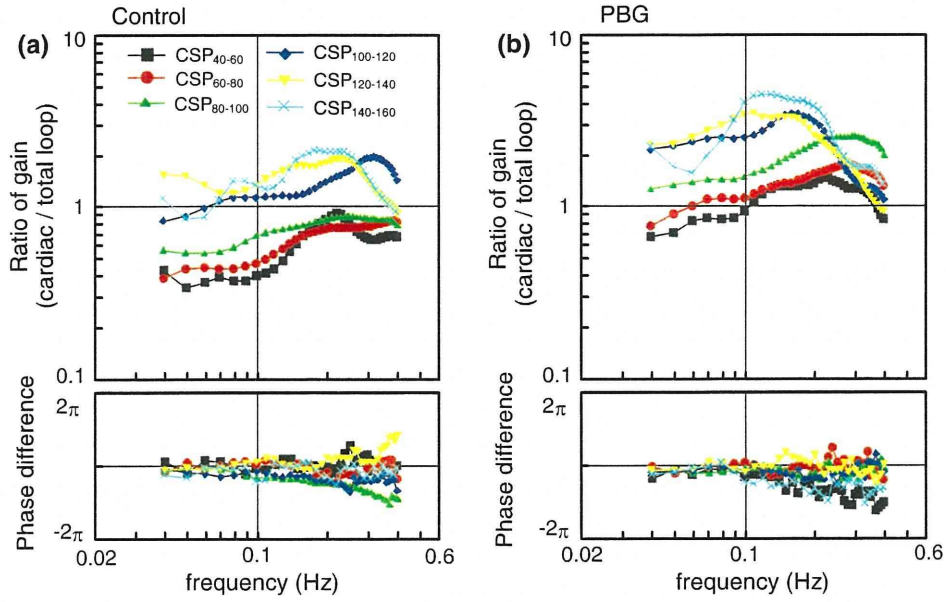

FIGURE 7. The ratio in the transfer functions of the cardiac baroreflex (CSP-HR) to the total loop (CSP-AP) (n = 8). The ratio of dynamic gain (*top*) and the phase difference (*bottom*). Control (a) and PBG (b) conditions.

transform that can adjust the analysis window at every frequency level and extract the localized data. When the mother wavelet is appropriately used for any purpose, the fields of the application of wavelet analysis might be extended. We used the traditional and reasonable Morlet function;[11,48,49] however, the comparison with other wavelet functions such as Mexican hat, Haar, and Daubechies[34] will be required in future studies. In addition, the convolutions within the transfer function of Eq. (3) may lose the temporal information; however, because the wavelet transform reflects the effect of reasonably changed time window, the gain and phase updated every 0.2 s can continuously express the representative property at the center point of the time window during the time-course change.

Physiological Perspective

The powers of the RSNA, AP, and HR responses to CSP changes showed maximum values at CSP_{80-100} change (Fig. 3b), which was almost consistent with AP_{OP} (94.3 and 99.7 mmHg) from static analysis. In contrast, the power responses at CSP_{40-60} and $CSP_{140-160}$ changes were lower than those at AP_{OP}, resulting from the nonlinear characteristics of the baroreflex around threshold and saturation to AP inputs as indicated by the static analysis. The gain and phase were revealed within the physiological range including nonlinear points in normal rabbits (Figs. 4 and 5). Whereas the static analysis cannot show the dynamic characteristics at higher frequencies (e.g. >0.01 Hz[18]), the proposed wavelet-based analysis

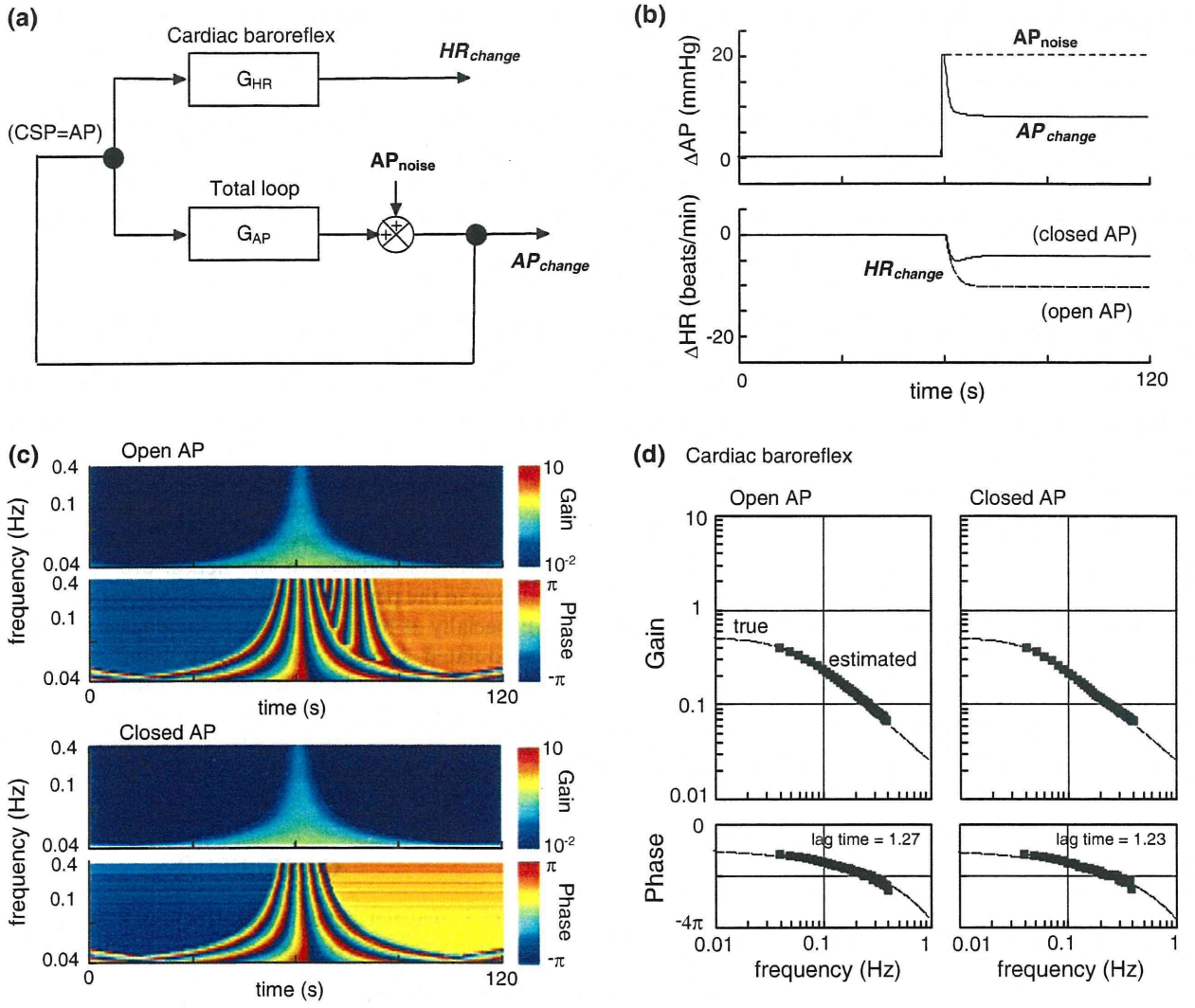

FIGURE 8. (a) Block diagram of cardiac baroreflex under closed-loop AP response. AP_{noise} indicates the external disturbance to AP. AP_{change} and HR_{change} show the actual changes of AP and HR. G_{AP} and G_{HR} are transfer functions under open loop responses in the total loop and cardiac baroreflex. (b) AP_{noise} of +20 mmHg as input and AP_{change} as output under the closed loop (*top*). HR responses under the open- and closed-loop AP changes (*bottom*). (c) Time-series transfer functions of cardiac baroreflex under open- and closed-loop AP changes. (d) Transfer functions of cardiac baroreflex estimated under the open (*left*) and closed (*right*) AP responses. Gain (*top*) and phase (*bottom*). Dotted lines, theoretical values. Squares, estimated values by our wavelet analysis.

could derive them from the same step input protocol, which may be able to reduce the number of experiments and duration of data acquisition.

Clinical Implications for Cardiac Patients

The wavelet-based system identification indicated a possibility to acquire pathophysiological understanding under various responses with cardiac diseases. The proposed analysis revealed that the dynamic characteristics in the total loop and neural arc were significantly attenuated at various pressure changes containing nonlinear points under PBG condition (Fig. 6 and Table 2), in addition to the previous studies.[18,20] The $G_{0.04}$ at AP_{OP} in Control (1.39 ± 0.15) was decreased to almost half during PBG condition (0.59 ± 0.09); it was attenuated to 1/3–1/4 times as small as that under PBG condition (0.39 ± 0.09) at low CSP_{40-60} change, which may be induced by the decrease of peripheral pump function in heart failure, suggesting the risk of further bluntness of baroreflex ability during the BJR.

In carotid-cardiac response, HR may be related to the assessment of AP regulation by the product of HR, stroke volume, and total peripheral resistance, rather than RR interval.[7,8] Because it may be difficult to evaluate the baroreflex to regulate AP under the carotid-sinus closed loop condition (i.e. CSP = AP), we

explored the possibility to evaluate the baroreflex dynamics from the HR response related to AP regulation, considering the dissociation between animal and human studies and applying the proposed method. The transfer functions of the cardiac baroreflex were similar to those of the total loop around the operating point (Fig. 7a). On the other hand, the dynamic characteristics in nonlinear CSP points and during the BJR were greater than those around the operating point in Control condition (Fig. 7b), suggesting the effect of cardiac sympathovagal activity. Next, to consider human baroreflex assessment, the dynamic transfer function was estimated by the closed-loop model response (Fig. 8), resulting in the effective assessment. Even when the system input is modulated by the nature of closed-loop response, it would be crucial to be able to estimate the dynamic baroreflex characteristics.

The spontaneous baroreflex method is commonly used in clinical assessments.[37] This method may have some limitations because of the highly complex and interconnected cardiovascular mechanisms in short-term AP regulation[27,40,43] and the unclear system input might induce the different pathophysiological understandings.[42] On the other hand, our focus was to explore the possibility of the evaluation of the baroreflex to regulate AP against great external disturbances in patients with cardiovascular diseases and unstable hemodynamics. To identify the system dynamics of the carotid-sinus baroreflex for AP regulation with sympathovagal activity,[51] this study improved the standard analyses, particularly considering the pure time delay. Using the transfer function corresponding to the independent step input frequency, the proposed analysis was able to indicate some novel aspects of the dynamic baroreflex properties during the BJR as mentioned above.

For clinical application, the other indexes (e.g. AP to muscle SNA response[14]) for AP regulation might be tested. In addition, in the time-course data, there are some effective methods such as complex demodulation method[13] based on the low pass filter, focusing on a frequency band such as LF and HF; it has good temporal resolution. However, the complex demodulation method might concentrate on the information of amplitude in a frequency band, not on each frequency level within the band. This limitation makes it impossible to perform the system identification in this study to reproduce the response corresponding to a wide frequency. Furthermore, the continuous estimation of the dynamics might connect to an effective index of the real-time control of hemodynamics such as an automated drug infusion system.[17,19]

Because we kept the bilateral vagi intact, low pressure baroreflexes from the cardiopulmonary region might have interacted with the arterial baroreflex, affecting estimation of carotid sinus baroreflex transfer functions. After the vagotomy, the dynamics from isolated aortic depressor nerve to AP responses was almost preserved and AP remained unchanged despite a HR decrease.[28,46] Our previous data of dynamic baroreflex properties with[20] and without[21] vagal nerves were compared. The dynamic characteristics of the total loop and cardiac baroreflex around the operating point were similar, whereas the corner frequency was slightly greater under intact vagal condition. Next, the static gain may be increased during the rising pressure protocol, compared with the falling one.[46] Hysteresis induced by the rising and falling pressure protocols may also modulate the dynamic baroreflex. However, the vagal effect of the cardiovascular receptors on the dynamics may not be large.[28] Third, the phases at lower or higher CSP changes in the transfer functions varied with the observed frequency because of nonlinear characteristics in the neural arc and the input power in the peripheral arc decreased by the neural arc. Especially at high frequencies, the phases appear to be modulated because of the step input showing low power with the high frequency. Finally, the simple models used for the simulations in this study have some limitations, such as a lack of information of nonparametric components or nonlinearity.[23]

CONCLUSIONS

The wavelet-based time-frequency analysis was capable of identifying the dynamic baroreflex properties over wide frequencies at various pressure levels both in normal and BJR conditions. Because the dynamic baroreflex properties to physiological pressure inputs as well as static characteristics can be simultaneously extracted from the short-term responses with background noise, the proposed method is potentially applicable to assess human dynamic baroreflex function under carotid-sinus closed-loop condition.

APPENDIX

Model Response of Arterial Baroreflex

We used the following model[15] as the carotid sinus open loop baroreflex for the simulation study (Figs. 1 and 2). The neural arc transfer function [$G_N(f)$] using a first-order high-pass filter can be expressed as

$$G_N(f) = -K_N\left(1 + \frac{f}{f_C}i\right)\exp(-2\pi f i L_N)$$

where f and i represent the frequency (Hz) and imaginary units, respectively; K_N is the neural arc gain; f_C is the frequency (Hz) for a derivative characteristic; L_N is lag time (s).

The peripheral arc transfer function [$G_P(f)$] using a second-order low-pass filter can be expressed as

$$G_P(f) = \frac{K_P}{1 + 2\zeta\frac{f}{f_N}i + \left(\frac{f}{f_N}i\right)^2} \exp(-2\pi f i L_P)$$

where K_P, f_N, ζ, and L_P represent the peripheral arc gain, natural frequency (Hz), damping ratio, and lag time (s), respectively.

The transfer function of the total baroreflex loop is expressed as the product of the neural and peripheral arc transfer functions.

$$G_{AP}(f) = G_N(f) \cdot G_P(f)$$

The gain and lag time of the total baroreflex loop is expressed as $K = K_N \cdot K_P$ and $L = L_N + L_P$. The parameters of the model response were set at $K = 1.0$, $f_C = 0.12$, $L_N = 0.55$, $f_N = 0.071$, $\zeta = 1.37$, and $L_P = 1.0$ according to previous data.[15]

Model of Baroreflex Under Closed-Loop AP Response

The baroreflex system under the closed-loop AP input to HR response was modeled (Fig. 8a).

$$HR_{change}(f) = G_{HR}(f) \cdot AP_{change}(f)$$

The pressure change [$AP_{change}(f)$] to the exogenous perturbation [$AP_{noise}(f)$] is the sum of the feedback signal and perturbation under closed-loop condition.[15] G_{HR} is the transfer function under the carotid sinus open loop in the cardiac baroreflex (CSP input and HR output).

$$AP_{change}(f) = G_{AP}(f) \cdot AP_{change}(f) + AP_{noise}(f)$$

Rearranging above equation with respect to $AP_{change}(f)$ yields

$$AP_{change}(f) = \frac{AP_{noise}(f)}{1 - G_{AP}(f)}$$

The time integral of the inverse Fourier transform of $AP_{change}(f)$ is the AP change to an exogenous step perturbation. G_{AP} is the transfer function under the carotid sinus open loop for the total baroreflex. The AP_{change} and HR_{change} can be simply observed by the monitoring system. The transfer function between the HR and AP responses was excluded because of the insignificant relationship as previously indicated.[22]

The transfer functions, G_{AP} and G_{HR}, were approximated using a first-order low-pass filter.

$$G(f) = \frac{-K}{\left(1 + \frac{f}{f_C}i\right)} \cdot \exp(-2\pi f i L)$$

The parameters of the transfer functions were set at $K = 1.03$, $f_C = 0.018$, and $L = 1.34$ for the total loop (Fig. 8a, G_{AP}); $K = 0.51$, $f_C = 0.049$, and $L = 1.14$ for the cardiac baroreflex (G_{HR}), according to previous data.[20]

ACKNOWLEDGMENTS

This study was supported by "Health and Labour Sciences Research Grant for Research on Advanced Medical Technology", "Health and Labour Sciences Research Grant for Research on Medical Devices for Analyzing, Supporting and Substituting the Function of Human Body", "Health and Labour Sciences Research Grant H18-Iryo-Ippan-023" from the Ministry of Health, Labour and Welfare of Japan, "Program for Promotion of Fundamental Studies in Health Science" from the National Institute of Biomedical Innovation, and "a Grant-in-Aid for Young Scientists (B)" from the Ministry of Education, Culture, Sports, Science and Technology of Japan (KAKENHI, 20700392).

REFERENCES

[1]Ando, S., H. R. Dajani, B. L. Senn, G. E. Newton, and J. S. Floras. Sympathetic alternans. Evidence for arterial baroreflex control of muscle sympathetic nerve activity in congestive heart failure. *Circulation* 95:316–319, 1997.

[2]Burgess, D. E., D. C. Randall, R. O. Speakman, and D. R. Brown. Coupling of sympathetic nerve traffic and BP at very low frequencies is mediated by large-amplitude events. *Am. J. Physiol. Regul. Integr. Comp. Physiol.* 284:R802–R810, 2003.

[3]Dampney, R. A. Functional organization of central pathways regulating the cardiovascular system. *Physiol. Rev.* 74:323–364, 1994.

[4]Davrath, L. R., Y. Goren, I. Pinhas, E. Toledo, and S. Akselrod. Early autonomic malfunction in normotensive individuals with a genetic predisposition to essential hypertension. *Am. J. Physiol. Heart Circ. Physiol.* 285:H1697–H1704, 2003.

[5]Eckberg, D. L., and T. A. Kuusela. Human vagal baroreflex sensitivity fluctuates widely and rhythmically at very low frequencies. *J. Physiol.* 567:1011–1019, 2005. doi:10.1113/jphysiol.2005.091090.

[6]Ellenbogen, K. A., P. K. Mohanty, S. Szentpetery, and M. D. Thames. Arterial baroreflex abnormalities in heart failure: reversal after orthotopic cardiac transplantation. *Circulation* 79:51–58, 1989.

[7]Fadel, P. J., S. Ogoh, D. M. Keller, and P. B. Raven. Recent insights into carotid baroreflex function in humans

using the variable pressure neck chamber. *Exp. Physiol.* 88:671–680, 2003. doi:10.1113/eph8802650.

[8]Fadel, P. J., M. Stromstad, D. W. Wray, S. A. Smith, P. B. Raven, and N. H. Secher. New insights into differential baroreflex control of heart rate in humans. *Am. J. Physiol. Heart Circ. Physiol.* 284:H735–H743, 2003.

[9]Glantz, S. A. Primer of Biostatistics. 4th ed. New York: McGraw Hill, 1997.

[10]Grassi, G., C. Turri, G. Seravalle, G. Bertinieri, A. Pierini, and G. Mancia. Effects of chronic clonidine administration on sympathetic nerve traffic and baroreflex function in heart failure. *Hypertension* 38:286–291, 2001. doi:10.1161/hy1201.096117.

[11]Grossmann, A., R. Kronland-Martinet, and J. Morlet. Reading and understanding continuous wavelets transforms. In: Wavelets, Time-Frequency Methods and Phase Space, edited by J. M. Combes, A. Grossmann, and P. Tchamitchian. Berlin: Springer, 1989, pp. 2–20.

[12]Guyton, A. C., T. G. Coleman, and H. J. Granger. Circulation: overall regulation. *Annu. Rev. Physiol.* 34:13–46, 1972. doi:10.1146/annurev.ph.34.030172.000305.

[13]Hayano, J., J. A. Taylor, S. Mukai, A. Okada, Y. Watanabe, K. Takata, and T. Fujinami. Assessment of frequency shifts in R-R interval variability and respiration with complex demodulation. *J. Appl. Physiol.* 77:2879–2888, 1994.

[14]Ichinose, M., M. Saito, N. Kondo, and T. Nishiyasu. Time-dependent modulation of arterial baroreflex control of muscle sympathetic nerve activity during isometric exercise in humans. *Am. J. Physiol. Heart Circ. Physiol.* 290:H1419–H1426, 2006. doi:10.1152/ajpheart.00847.2005.

[15]Ikeda, Y., T. Kawada, M. Sugimachi, O. Kawaguchi, T. Shishido, T. Sato, H. Miyano, W. Matsuura, J. Alexander, Jr., and K. Sunagawa. Neural arc of baroreflex optimizes dynamic pressure regulation in achieving both stability and quickness. *Am. J. Physiol. Heart Circ. Physiol.* 271:H882–H890, 1996.

[16]Jordan, J., H. R. Toka, K. Heusser, O. Toka, J. R. Shannon, J. Tank, A. Diedrich, C. Stabroth, M. Stoffels, R. Naraghi, W. Oelkers, H. Schuster, H. P. Schobel, H. Haller, and F. C. Luft. Severely impaired baroreflex-buffering in patients with monogenic hypertension and neurovascular contact. *Circulation* 102:2611–2618, 2000.

[17]Kashihara, K. Automatic regulation of hemodynamic variables in acute heart failure by a multiple adaptive predictive controller based on neural networks. *Ann. Biomed. Eng.* 34:1846–1869, 2006. doi:10.1007/s10439-006-9190-9.

[18]Kashihara, K., T. Kawada, M. Li, M. Sugimachi, and K. Sunagawa. Bezold-Jarisch reflex induced by phenylbiguanide lowers arterial pressure mainly via the downward shift of the baroreflex neural arc. *Jpn. J. Physiol.* 54:395–404, 2004. doi:10.2170/jjphysiol.54.395.

[19]Kashihara, K., T. Kawada, K. Uemura, M. Sugimachi, and K. Sunagawa. Adaptive predictive control of arterial blood pressure based on a neural network during acute hypotension. *Ann. Biomed. Eng.* 32:1365–1383, 2004. doi:10.1114/B:ABME.0000042225.19806.34.

[20]Kashihara, K., T. Kawada, Y. Yanagiya, K. Uemura, M. Inagaki, H. Takaki, M. Sugimachi, and K. Sunagawa. Bezold-Jarisch reflex attenuates dynamic gain of baroreflex neural arc. *Am. J. Physiol. Heart Circ. Physiol.* 285:H833–H840, 2003.

[21]Kashihara, K., Y. Takahashi, K. Chatani, T. Kawada, C. Zheng, M. Li, M. Sugimachi, and K. Sunagawa. Intravenous angiotensin II does not affect dynamic baroreflex characteristics of the neural or peripheral arc. *Jpn. J. Physiol.* 53:135–143, 2003. doi:10.2170/jjphysiol.53.135.

[22]Kawada, T., T. Miyamoto, K. Uemura, K. Kashihara, A. Kamiya, M. Sugimachi, and K. Sunagawa. Effects of neuronal norepinephrine uptake blockade on baroreflex neural and peripheral arc transfer characteristics. *Am. J. Physiol. Regul. Integr. Comp. Physiol.* 286:R1110–1120, 2004. doi:10.1152/ajpregu.00527.2003.

[23]Kawada, T., Y. Yanagiya, K. Uemura, T. Miyamoto, C. Zheng, M. Li, M. Sugimachi, and K. Sunagawa. Input-size dependence of the baroreflex neural arc transfer characteristics. *Am. J. Physiol. Heart Circ. Physiol.* 284:H404–H415, 2003.

[24]Kent, B. B., J. W. Drane, B. Blumenstein, and J. W. Manning. A mathematical model to assess changes in the baroreceptor reflex. *Cardiology* 57:295–310, 1972.

[25]Landesberg, G., D. Adam, Y. Berlatzky, and S. Akselrod. Step baroreflex response in awake patients undergoing carotid surgery: time- and frequency-domain analysis. *Am. J. Physiol.* 274:H1590–H1597, 1998.

[26]Lee, D. Coherent oscillations in neuronal activity of the supplementary motor area during a visuomotor task. *J. Neurosci.* 23:6798–6809, 2003.

[27]Lipman, R. D., J. K. Salisbury, and J. A. Taylor. Spontaneous indices are inconsistent with arterial baroreflex gain. *Hypertension* 42:481–487, 2003. doi:10.1161/01.HYP.0000091370.83602.E6.

[28]Liu, H. K., S. J. Guild, J. V. Ringwood, C. J. Barrett, B. L. Leonard, S. K. Nguang, M. A. Navakatikyan, and S. C. Malpas. Dynamic baroreflex control of blood pressure: influence of the heart vs. peripheral resistance. *Am. J. Physiol. Regul. Integr. Comp. Physiol.* 283:R533–R542, 2002.

[29]Lucini, D., M. Pagani, G. S. Mela, and A. Malliani. Sympathetic restraint of baroreflex control of heart period in normotensive and hypertensive subjects. *Clin. Sci. (Lond.)* 86:547–556, 1994.

[30]Malliani, A., M. Pagani, F. Lombardi, and S. Cerutti. Cardiovascular neural regulation explored in the frequency domain. *Circulation* 84:482–492, 1991.

[31]Marmarelis, P. Z., and V. Z. Marmarelis. The white noise method in system identification. In: Analysis of Physiological Systems. New York: Plenum, 1978, pp. 131–221.

[32]Masaki, H., T. Imaizumi, Y. Harasawa, and A. Takeshita. Dynamic arterial baroreflex in rabbits with heart failure induced by rapid pacing. *Am. J. Physiol.* 267:H92–H99, 1994.

[33]Mohrman, D. E., and L. J. Heller. Cardiovascular Physiology. 4th ed. New York: McGraw-Hill, 1997.

[34]Motard, R. L., and B. Joseph. Wavelet Applications in Chemical Engineering. Boston: Kluwer Academic Publishers, 1994.

[35]Munakata, M., Y. Imai, H. Takagi, M. Nakao, M. Yamamoto, and K. Abe. Altered frequency-dependent characteristics of the cardiac baroreflex in essential hypertension. *J. Auton. Nerv. Syst.* 49:33–45, 1994. doi:10.1016/0165-1838(94)90018-3.

[36]Osculati, G., G. Grassi, C. Giannattasio, G. Seravalle, F. Valagussa, A. Zanchetti, and G. Mancia. Early alterations of the baroreceptor control of heart rate in patients with acute myocardial infarction. *Circulation* 81:939–948, 1990.

[37]Parati, G., M. DiRienzo, and G. Mancia. Dynamic modulation of baroreflex sensitivity in health and disease. *Ann. NY Acad. Sci.* 940:469–487, 2001.

[38]Parati, G., J. P. Saul, and P. Castiglioni. Assessing arterial baroreflex control of heart rate: new perspectives. *J. Hypertens.* 22:1259–1263, 2004. doi:10.1097/01.hjh.0000125469.35523.32.

[39]Parmer, R. J., J. H. Cervenka, and R. A. Stone. Baroreflex sensitivity and heredity in essential hypertension. *Circulation* 85:497–503, 1992.

[40]Persson, P. B., M. DiRienzo, P. Castiglioni, C. Cerutti, M. Pagani, N. Honzikova, S. Akselrod, and G. Parati. Time versus frequency domain techniques for assessing baroreflex sensitivity. *J. Hypertens.* 19:1699–1705, 2001. doi:10.1097/00004872-200110000-00001.

[41]Pinna, G. D., R. Maestri, G. Raczak, and M. T. La Rovere. Measuring baroreflex sensitivity from the gain function between arterial pressure and heart period. *Clin. Sci. (Lond.)* 103:81–88, 2002.

[42]Pitzalis, M. V., F. Mastropasqua, A. Passantino, F. Massari, L. Ligurgo, C. Forleo, C. Balducci, F. Lombardi, and P. Rizzon. Comparison between noninvasive indices of baroreceptor sensitivity and the phenylephrine method in post-myocardial infarction patients. *Circulation* 97:1362–1367, 1998.

[43]Porta, A., G. Baselli, O. Rimoldi, A. Malliani, and M. Pagani. Assessing baroreflex gain from spontaneous variability in conscious dogs: role of causality and respiration. *Am. J. Physiol. Heart Circ. Physiol.* 279:H2558–H2567, 2000.

[44]Radaelli, A., L. Bernardi, F. Valle, S. Leuzzi, F. Salvucci, L. Pedrotti, E. Marchesi, G. Finardi, and P. Sleight. Cardiovascular autonomic modulation in essential hypertension. Effect of tilting. *Hypertension* 24:556–563, 1994.

[45]Rudas, L., A. A. Crossman, C. A. Morillo, J. R. Halliwill, K. U. Tahvanainen, T. A. Kuusela, and D. L. Eckberg. Human sympathetic and vagal baroreflex responses to sequential nitroprusside and phenylephrine. *Am. J. Physiol.* 276:H1691–H1698, 1999.

[46]Sagawa, K. Baroreflex control of systemic arterial pressure and vascular bed. In: Handbook of Physiology. The Cardiovascular System. Peripheral Circulation and Organ Blood Flow, sect. 2, vol. III, pt. 2, chap. 14. Bethesda, MD: Am. Physiol. Soc., 1983, pp. 453–496.

[47]Sato, T., T. Kawada, M. Inagaki, T. Shishido, H. Takaki, M. Sugimachi, and K. Sunagawa. New analytic framework for understanding sympathetic baroreflex control of arterial pressure. *Am. J. Physiol.* 276:H2251–H2261, 1999.

[48]Sinkkonen, J., H. Tiitinen, and R. Naatanen. Gabor filters: an informative way for analysing event-related brain activity. *J. Neurosci. Methods* 56:99–104, 1995. doi:10.1016/0165-0270(94)00111-S.

[49]Tallon-Baudry, C., O. Bertrand, C. Delpuech, and J. Pernier. Stimulus specificity of phase-locked and non-phase-locked 40 Hz visual responses in human. *J. Neurosci.* 16:4240–4249, 1996.

[50]Toledo, E., O. Gurevitz, H. Hod, M. Eldar, and S. Akselrod. Wavelet analysis of instantaneous heart rate: a study of autonomic control during thrombolysis. *Am. J. Physiol. Regul. Integr. Comp. Physiol.* 284:R1079–R1091, 2003.

[51]Westerhof, B. E., J. Gisolf, J. M. Karemaker, K. H. Wesseling, N. H. Secher, and J. J. van Lieshout. Time course analysis of baroreflex sensitivity during postural stress. *Am. J. Physiol. Heart Circ. Physiol.* 291:H2864–H2874, 2006. doi:10.1152/ajpheart.01024.2005.

[52]Zhang, R., K. Behbehani, C. G. Crandall, J. H. Zuckerman, and B. D. Levine. Dynamic regulation of heart rate during acute hypotension: new insight into baroreflex function. *Am. J. Physiol. Heart Circ. Physiol.* 280:H407–H419, 2001.

Am J Physiol Heart Circ Physiol 296: H1666–H1674, 2009.
First published February 27, 2009; doi:10.1152/ajpheart.01041.2008.

Angiotensin II disproportionally attenuates dynamic vagal and sympathetic heart rate controls

Toru Kawada,[1] Masaki Mizuno,[1] Shuji Shimizu,[2] Kazunori Uemura,[1] Atsunori Kamiya,[1] and Masaru Sugimachi[1]

[1]*Department of Cardiovascular Dynamics, Advanced Medical Engineering Center, National Cardiovascular Center Research Institute, Osaka and* [2]*Japan Association for the Advancement of Medical Equipment, Tokyo, Japan*

Submitted 29 September 2008; accepted in final form 25 February 2009

Kawada T, Mizuno M, Shimizu S, Uemura K, Kamiya A, Sugimachi M. Angiotensin II disproportionally attenuates dynamic vagal and sympathetic heart rate controls. *Am J Physiol Heart Circ Physiol* 296: H1666–H1674, 2009. First published February 27, 2009; doi:10.1152/ajpheart.01041.2008.—To better understand the pathophysiological role of angiotensin II (ANG II) in the dynamic autonomic regulation of heart rate (HR), we examined the effects of intravenous administration of ANG II (10 $\mu g \cdot kg^{-1} \cdot h^{-1}$) on the transfer function from vagal or sympathetic nerve stimulation to HR in anesthetized rabbits with sinoaortic denervation and vagotomy. In the vagal stimulation group (n = 7), we stimulated the right vagal nerve for 10 min using binary white noise (0–10 Hz). The transfer function from vagal stimulation to HR approximated a first-order low-pass filter with pure delay. ANG II attenuated the dynamic gain from 7.6 ± 0.9 to 5.8 ± 0.9 beats·$min^{-1} \cdot Hz^{-1}$ (means ± SD; $P <$ 0.01) without affecting the corner frequency or pure delay. In the sympathetic stimulation group (n = 7), we stimulated the right postganglionic cardiac sympathetic nerve for 20 min using binary white noise (0–5 Hz). The transfer function from sympathetic stimulation to HR approximated a second-order low-pass filter with pure delay. ANG II slightly attenuated the dynamic gain from 10.8 ± 2.6 to 10.2 ± 3.1 beats·$min^{-1} \cdot Hz^{-1}$ (P = 0.049) without affecting the natural frequency, damping ratio, or pure delay. The disproportional suppression of the dynamic vagal and sympathetic regulation of HR would result in a relative sympathetic predominance in the presence of ANG II. The reduced high-frequency component of HR variability in patients with cardiovascular diseases, such as myocardial infarction and heart failure, may be explained in part by the peripheral effects of ANG II on the dynamic autonomic regulation of HR.

systems analysis; transfer function; heart rate variability; cardiac sympathetic nerve activity; rabbit

AUTONOMIC NERVOUS ACTIVITY changes dynamically during daily activity, and thus the dynamic heart rate (HR) regulation by the autonomic nervous system is physiologically important. The high-frequency (HF) component of HR variability (HRV) is thought to reflect primarily vagal nerve activity, because the vagal nerve can change the HR more quickly than the sympathetic nerve (1, 3, 14, 34). This does not mean, however, that the sympathetic system cannot affect the HF component. For example, an increase in background sympathetic tone augments the HR response to vagal stimulation, an effect that has been referred to as accentuated antagonism (20). In accordance with accentuated antagonism, selective cardiac sympathetic nerve stimulation augments the dynamic HR response to vagal stimulation (14). On the other hand, high plasma concentration of norepinephrine (NE) with no direct activation of the cardiac sympathetic nerve attenuates the dynamic HR response to vagal stimulation via an α-adrenergic mechanism (24). These results suggest that the sympathetic system can influence the HF component via complex interactions with the vagal system.

During systemic sympathetic activation, the renin-angiotensin system is activated through stimulation of β_1-adrenergic receptors on juxtaglomerular granular cells (8, 12). In such conditions as hypertension, myocardial ischemia, and heart failure, the renin-angiotensin system and the sympathetic nervous system are both activated (9, 35). Previous studies demonstrated that acute intravenous or intracerebroventricular administration (32) or chronic intravenous administration of angiotensin II (ANG II) modified the baroreflex control of HR in rabbits (5), possibly via a decrease in vagal tone and an increase in sympathetic tone to the heart. In the present study, we focused on the peripheral effects of ANG II and examined the effects of intravenous ANG II on the dynamic HR response to vagal or postganglionic cardiac sympathetic nerve stimulation. In a previous study from our laboratory where anesthetized cats were used, intravenous ANG II (10 $\mu g \cdot kg^{-1} \cdot h^{-1}$) attenuated myocardial interstitial acetylcholine (ACh) release in response to vagal nerve stimulation (17); therefore, we hypothesized that intravenous ANG II at this dose would attenuate the dynamic HR response to vagal nerve stimulation. On the other hand, a previous study from our laboratory where anesthetized rabbits were used demonstrated that intravenous ANG II at a similar dose of 6 $\mu g \cdot kg^{-1} \cdot h^{-1}$ did not affect the peripheral arc transfer function estimated between renal sympathetic nerve activity and arterial pressure (AP) (13). Accordingly, we hypothesized that intravenous administration of ANG II would not modulate the dynamic sympathetic control of HR significantly. We focused on the relative effects of ANG II on the vagal and sympathetic HR regulations because the balance between vagal and sympathetic nerve activities would be a key to understanding the pathophysiology of several cardiovascular diseases.

MATERIALS AND METHODS

Surgical preparations. Animal care was performed in accordance with *Guideline Principles for the Care and Use of Animals in the Field of Physiological Sciences*, which has been approved by the Physiological Society of Japan. All experimental protocols were reviewed and approved by the Animal Subjects Committee at the National Cardiovascular Center. Twenty-one Japanese white rabbits weighing 2.4–3.4 kg were anesthetized with intravenous injections (2 ml/kg) of a mixture of urethane (250 mg/ml) and α-chloralose (40 mg/ml) and mechanically ventilated with oxygen-enriched room air. A double-lumen catheter was inserted into the right femoral vein, and a supplemental dose of the anesthetics was given continuously (0.5–1.0

Address for reprint requests and other correspondence: T. Kawada, Dept. of Cardiovascular Dynamics, Advanced Medical Engineering Center, National Cardiovascular Center Research Institute, 5-7-1 Fujishirodai, Suita, Osaka 565-8565, Japan (e-mail: torukawa@res.ncvc.go.jp).

$ml \cdot kg^{-1} \cdot h^{-1}$). AP was monitored using a micromanometer catheter (Millar Instruments, Houston, TX) inserted into the right femoral artery. HR was determined from the electrocardiogram using a cardiotachometer. Sinoaortic denervation and vagotomy were performed bilaterally to minimize reflex changes in efferent sympathetic nerve activity. The left and right cardiac sympathetic nerves were exposed using a midline thoracotomy and sectioned (16). In the vagal stimulation group, a pair of bipolar stainless steel wire electrodes was attached to the cardiac end of the sectioned right vagal nerve for stimulation. A pair of stainless steel wire electrodes was attached to the proximal end of the sectioned right cardiac sympathetic nerve for recording efferent cardiac sympathetic nerve activity (CSNA). In the sympathetic stimulation group, a pair of bipolar stainless steel wire electrodes was attached to the cardiac end of the sectioned right sympathetic nerve for stimulation. Efferent CSNA was recorded from the proximal end of the sectioned left cardiac sympathetic nerve. The preamplified nerve signal was band-pass filtered between 150 and 1,000 Hz. The signal was then full-wave rectified and low-pass filtered with a cut-off frequency of 30 Hz to quantify the nerve activity. Both the stimulation and recording electrodes were fixed to the nerve by addition-curing silicone glue (Kwik-Sil; World Precision Instruments, Sarasota, FL). We confirmed that the recorded CSNA was mainly postganglionic by observing the disappearance of CSNA following intravenous administration of hexamethonium bromide (50 mg/kg) at the end of each experiment. The body temperature of the animal was maintained at 38°C with a heating pad throughout the experiment.

Protocols. In the vagal stimulation group ($n = 7$), the stimulation amplitude was adjusted (3–6 V) in each animal to yield a HR decrease of ~50 beats/min at 5-Hz tonic stimulation with a pulse duration of 2 ms. To estimate the transfer function from vagal stimulation to HR, a random vagal stimulus was applied for 10 min by altering the stimulus command every 500 ms at either 0 or 10 Hz according to a binary white noise signal. The input power spectral density was relatively constant up to 1 Hz, which covered the upper frequency range of interest with respect to the vagal transfer function in rabbits (26).

In the sympathetic stimulation group ($n = 7$), the stimulation amplitude was adjusted (1–3 V) in each animal to yield a HR increase of ~50 beats/min at 5-Hz tonic stimulation with a pulse duration of 2 ms. To estimate the transfer function from sympathetic stimulation to HR, a random sympathetic stimulus was applied for 20 min by altering the stimulus command every 2 s at either 0 or 5 Hz according to a binary white noise signal. The input power spectral density was relatively constant up to 0.25 Hz, which covered the upper frequency range of interest with respect to the sympathetic transfer function in rabbits (15).

In both the vagal stimulation and sympathetic stimulation groups, the dynamic HR response to nerve stimulation was first recorded under conditions of continuous intravenous infusion of physiological saline solution ($1\ ml \cdot kg^{-1} \cdot h^{-1}$). After the control data were recorded, nerve stimulation was stopped and ANG II was intravenously administered at $10\ \mu g \cdot kg^{-1} \cdot h^{-1}$ ($1\ ml \cdot kg^{-1} \cdot h^{-1}$ of 10 μg/ml solution) instead of the physiological saline solution. After 15 min, we repeated the random stimulation of the vagal or sympathetic nerve while continuing the intravenous injection of ANG II. We used the same binary white noise sequence for the control and ANG II conditions in each animal and changed the sequence for different animals.

In a supplemental protocol ($n = 7$), we examined the time effect on the estimation of the sympathetic transfer function. The 20-min random sympathetic stimulation was repeated twice with an intervening interval of more than 20 min.

Data analysis. Data were digitized at 200 Hz using a 16-bit analog-to-digital converter and stored on the hard disk of a dedicated laboratory computer system. Prestimulation values of HR, AP, and CSNA were calculated by averaging data obtained during the 10 s immediately before nerve stimulation. The mean HR and AP values in response to nerve stimulation were calculated by averaging data obtained during the nerve stimulation period. The mean level of CSNA during the nerve stimulation period was not evaluated because contamination from stimulation artifacts could not be completely eliminated.

The transfer function from nerve stimulation to the HR response was estimated as follows. The input-output data pairs of nerve stimulation and HR were resampled at 10 Hz. To avoid the initial transition from no stimulation to random stimulation biased the transfer function estimation, data were processed only from 2 min after the initiation of random stimulation. In the vagal stimulation group, the data were divided into eight segments of 1,024 data points that half-overlapped with neighboring segments. In the sympathetic stimulation group, the data were divided into eight segments of 2,048 data points that half-overlapped with neighboring segments. For each segment, a linear trend was subtracted and a Hanning window was applied. We then performed a fast Fourier transformation to obtain the frequency spectra of the stimulation command [$X(f)$] and HR [$HR(f)$] (4). We calculated ensemble averages of the power spectral densities of the stimulation command [$S_{X \cdot X}(f)$] and HR [$S_{HR \cdot HR}(f)$] and the cross spectral density between the two signals [$S_{HR \cdot X}(f)$]. Finally, we obtained the transfer function [$H(f)$] from the nerve stimulation to HR response using the following equation (23):

$$H(f) = \frac{S_{HR \cdot X}(f)}{S_{X \cdot X}(f)}$$

To quantify the linear dependence of the HR response to vagal or sympathetic nerve stimulation, we estimated the magnitude-squared coherence function [$Coh(f)$] using the following equation (23):

$$Coh(f) = \frac{|S_{HR \cdot X}(f)|^2}{S_{X \cdot X}(f) \cdot S_{HR \cdot HR}(f)}$$

The coherence function ranges zero and unity and indicates a frequency-domain measure of linear dependence between input and output variables.

Because previous studies found that the transfer function from vagal stimulation to HR approximated a first-order low-pass filter with pure delay (14, 24), we determined the parameters of the vagal transfer function using the following model:

$$H_{vagus}(f) = -\frac{K}{1 + \frac{f}{f_C} j} e^{-2\pi f j L}$$

where K is dynamic gain (in $beats \cdot min^{-1} \cdot Hz^{-1}$), f_C is the corner frequency (in Hz), and L is pure delay (in s). Variables f and j represent frequency and an imaginary unit, respectively. The minus sign in the right side of the equation corresponds to the negative HR response to vagal stimulation.

Because previous studies suggested that the transfer function from sympathetic stimulation to HR approximated a second-order low-pass filter with pure delay (14, 28), we determined the parameters of the sympathetic transfer function using the following model:

$$H_{symp}(f) = \frac{K}{1 + 2\zeta \frac{f}{f_N} j + \left(\frac{f}{f_N} j\right)^2} e^{-2\pi f j L}$$

where K is dynamic gain (in $beats \cdot min^{-1} \cdot Hz^{-1}$), f_N is the natural frequency (in Hz), ζ is the damping ratio, and L is pure delay (in s).

Because deviation of the model transfer function [$H_{model}(f)$] from the estimated transfer function [$H_{est}(f)$] would affect the transfer function parameters, we assessed the goodness of fit using the following equation:

$$\text{Goodness of Fit (\%)} = 100 \times \left[1 - \left(\sum_{m=1}^{N} \frac{|H_{model}(f) - H_{est}(f)|^2}{m} \right) \Big/ \left(\sum_{m=1}^{N} \frac{|H_{est}(f)|^2}{m} \right) \right]$$

$$f = f_0 \times m$$

where f_0, m, and N represent the fundamental frequency of the Fourier transformation, a frequency index, and the number of data points used for the fitting, respectively. When $H_{model}(f)$ is zero for all of the frequencies, the goodness of fit is zero. When $H_{model}(f)$ equals $H_{est}(f)$ for all of the frequencies, the goodness of fit is 100%.

To facilitate intuitive understanding of the dynamic characteristics described by the transfer function (see Appendix A for details), we calculated the step response from the corresponding transfer function as follows. An impulse response of the system was calculated using the inverse Fourier transformation of the estimated transfer function. The step response was then obtained from the time integral of the impulse response. The steady-state response was calculated by averaging the last 10 s of data from the step response. The 80% rise time for the sympathetic step response or the 80% fall time for the vagal step response was estimated as the time at which the step response reached 80% of the steady-state response.

Statistics. All data are presented as means and SD values. Mean values of HR, AP, and CSNA as well as parameters of the transfer functions and step responses were compared between the control and ANG II conditions using paired *t*-tests. Differences were considered significant when $P < 0.05$ (11).

RESULTS

Typical recordings of the vagal stimulation command, HR, and AP obtained under control and ANG II conditions are shown in Fig. 1*A*. The random vagal stimulation began at 60 s. The HR decreased in response to the random vagal stimulation. ANG II, which did not affect the prestimulation baseline HR, attenuated the magnitude of the vagal stimulation-induced variations in HR. ANG II increased the AP both before and during the vagal stimulation. ANG II did not change the prestimulation or poststimulation CSNA (Fig. 1*B*).

As shown in Table 1, ANG II did not affect the mean HR before stimulation of the vagal nerve, whereas it significantly increased the mean HR during the vagal stimulation period. ANG II attenuated the reduction in HR, which was calculated as the difference between the prestimulation HR and the mean HR observed during the vagal stimulation period. ANG II significantly increased the mean AP both before and during the vagal stimulation period. ANG II did not affect the mean level of pre- or poststimulation CSNA significantly.

Figure 2*A* illustrates the averaged transfer functions from vagal stimulation to HR obtained under the control and ANG II conditions. In the gain plots, the transfer gain was relatively constant for frequencies below 0.1 Hz and decreased as the frequency increased above 0.1 Hz. ANG II decreased the transfer gain for all of the investigated frequencies, resulting in

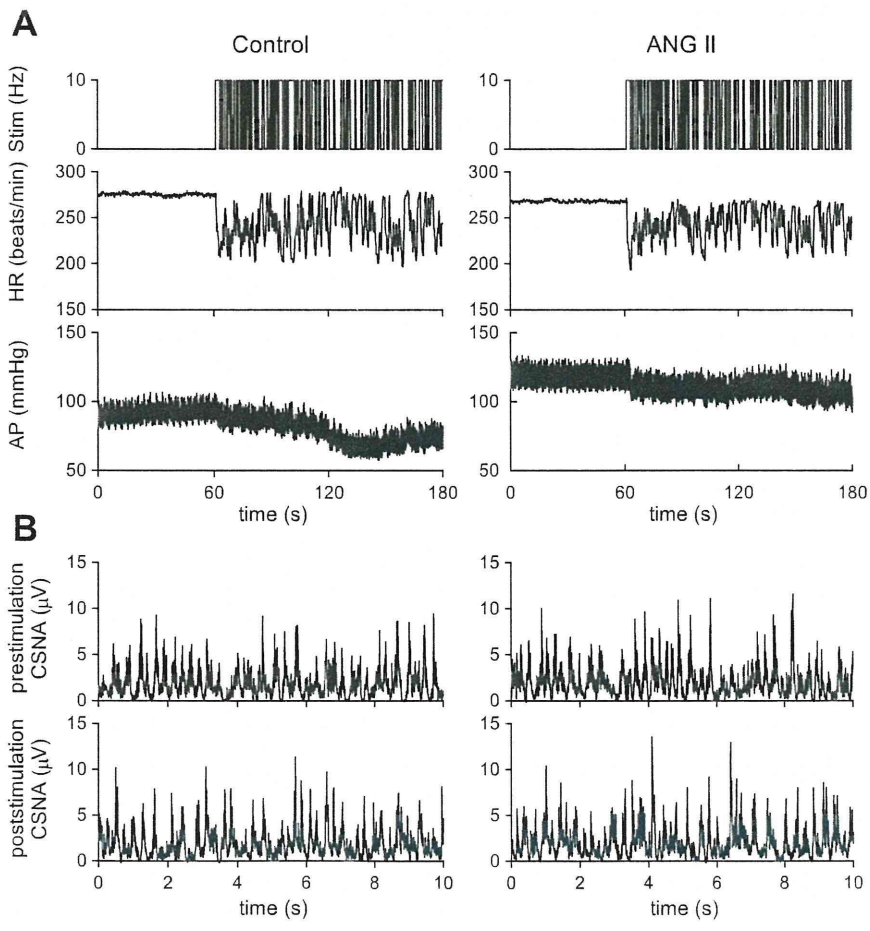

Fig. 1. *A*: representative recordings of vagal nerve stimulation (Stim), the heart rate (HR), and arterial pressure (AP). The *left* and *right* panels show recordings obtained before and during intravenous administration of angiotensin II (ANG II; 10 $\mu g \cdot kg^{-1} \cdot h^{-1}$), respectively. The amplitude of the HR variation in response to vagal stimulation was smaller in the presence of ANG II compared with results obtained without ANG II. *B*: representative recordings of cardiac sympathetic nerve activity (CSNA) under prestimulation baseline and poststimulation conditions. ANG II did not affect the CSNA significantly.

Table 1. *Mean values for HR, AP, and CSNA obtained using the vagal stimulation protocol*

	Control	ANG II	*P* Value
HR, beats/min			
Prestimulation	278±21	281±31	0.60
During stimulation	232±19	245±26*	0.046
Difference‡	−46±6	−37±10†	0.0017
AP, mmHg			
Prestimulation	91±23	127±17†	0.0057
During stimulation	85±24	118±19†	0.0055
Difference‡	−6.3±9.2	−9.2±8.6	0.34
CSNA, μV			
Prestimulation	1.21±0.38 (100%)	1.19±0.46 (98±15%)	0.82
Poststimulation	1.27±0.42 (105±8%)	1.20±0.55 (98±27%)	0.59

Data are means ± SD values; $n = 7$. HR, heart rate; AP, arterial pressure; CSNA, cardiac sympathetic nerve activity. ‡The difference was calculated by subtracting the prestimulation value from the value obtained during the vagal stimulation period in each animal. *$P < 0.05$ and †$P < 0.01$ based on a paired *t*-test. Exact *P* values are also shown.

a parallel downward shift in the gain plot. In the phase plots, the phase approached $-\pi$ radians at 0.01 Hz and the lag became larger as the frequency increased. ANG II did not alter the phase characteristics significantly. In the coherence plots, the coherence value was close to unity in the frequency range from 0.01 to 0.8 Hz. The sharp variation around 0.6 Hz corresponds to the frequency of the artificial ventilation. Figure 2*B* depicts the HR step responses calculated from the corresponding transfer functions. ANG II significantly attenuated the steady-state response without affecting the response speed.

As shown in Table 2, ANG II significantly attenuated the dynamic gain of the vagal transfer function to 76.1 ± 8.5% of the control value without affecting the corner frequency or pure delay. The goodness of fit to the first-order low-pass filter did not differ between the control and ANG II conditions. In the HR step response, ANG II significantly attenuated the steady-state response without affecting the 80% fall time.

Typical recordings of the sympathetic stimulation command, HR, and AP obtained under control and ANG II conditions are shown in Fig. 3*A*. The random sympathetic stimulation began at 60 s. HR increased in response to random sympathetic stimulation. ANG II did not affect the prestimulation baseline HR. The magnitude of the HR variation in response to sympathetic stimulation did not change significantly. ANG II increased the AP both before and during the sympathetic stimulation. ANG II did not change the pre- or poststimulation CSNA significantly (Fig. 3*B*).

As shown in Table 3, ANG II did not affect the mean HR before or during the period of sympathetic stimulation. ANG II did not affect the increase in HR, calculated as the difference between the prestimulation HR and the mean HR in response to sympathetic stimulation. ANG II significantly increased the mean AP both before and during the sympathetic stimulation period. ANG II did not affect the mean level of pre- or poststimulation CSNA significantly.

Figure 4*A* illustrates the averaged transfer functions from sympathetic stimulation to HR obtained under control and ANG II conditions. In the gain plots, the transfer gain decreased as the frequency increased. ANG II did not change the transfer gain markedly. In the phase plots, the phase approached zero radians at 0.01 Hz and increasingly lagged as the frequency increased. ANG II did not affect the phase characteristics significantly. The coherence value was above 0.9 for the frequency range below 0.1 Hz and decreased in the frequency range above 0.1 Hz. Figure 4*B* depicts the HR step responses calculated from the corresponding transfer functions. ANG II did not affect the steady-state response or the response speed.

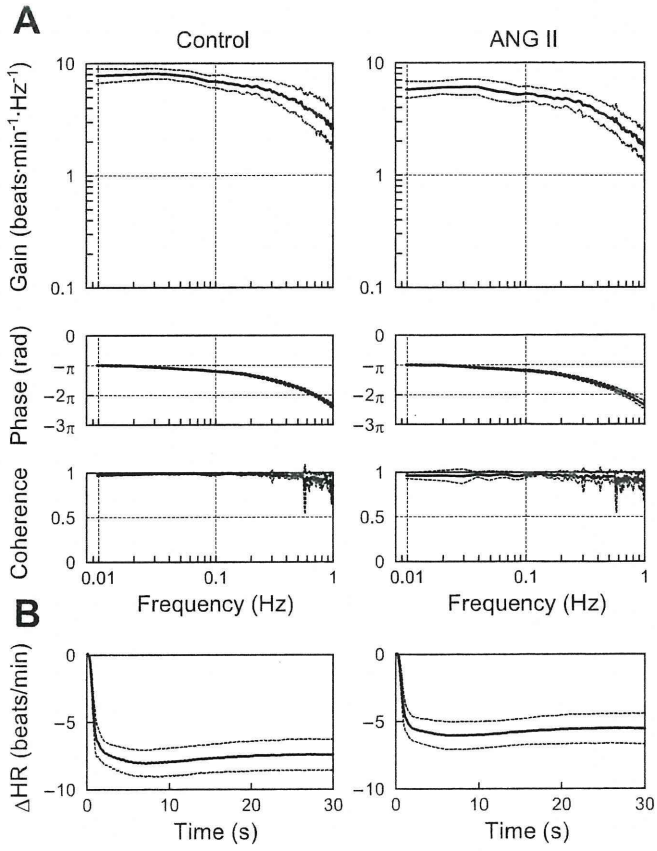

Fig. 2. *A*: averaged transfer functions from vagal nerve stimulation to the HR response obtained before and during intravenous administration of ANG II. Gain plots (*top*), phase plots (*middle*), and coherence plots (*bottom*) are shown. ANG II caused a parallel downward shift in the gain plot. ANG II did not affect the phase plot or coherence plot significantly. *B*: step responses of the HR to a unit change in the vagal stimulation calculated from the corresponding transfer functions. ANG II significantly attenuated the step response of the HR. ΔHR, changes in heart rate. Solid lines indicate mean, and dashed lines indicate mean ± SD.

Table 2. *Effects of ANG II on the parameters of the transfer function and the step response relating to the dynamic vagal control of HR*

	Control	ANG II	*P* Value
Dynamic gain, beats·min^{-1}·Hz^{-1}	7.6±0.9	5.8±0.9*	0.00042
Corner frequency, Hz	0.39±0.12	0.36±0.10	0.12
Pure delay, s	0.48±0.04	0.47±0.06	0.82
Goodness of fit, %	98.8±0.4	98.6±0.8	0.63
Steady-state response, beats/min	−7.4±1.1	−5.6±1.1*	0.0011
80% Fall time	1.31±0.31	1.33±0.37	0.60

Data are means ± SD values; $n = 7$. *$P < 0.01$ based on a paired *t*-test. Exact *P* values are also shown.

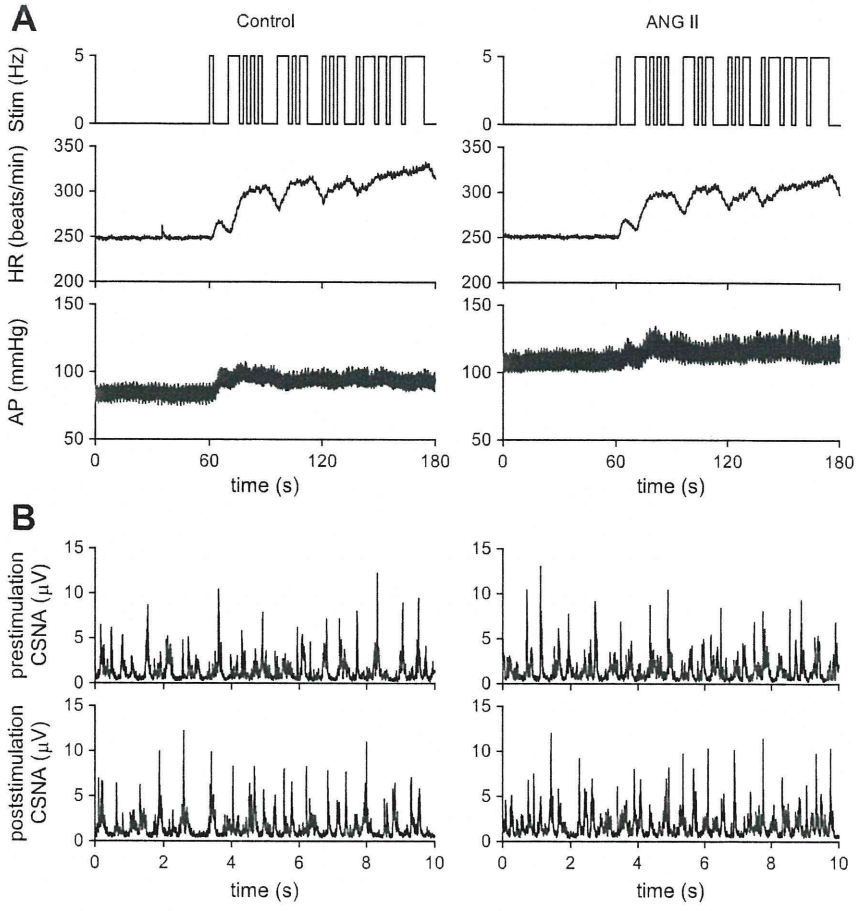

Fig. 3. *A*: representative recordings of cardiac sympathetic nerve stimulation (Stim), HR, and AP. The *left* and *right* panels show the recordings before and during intravenous administration of ANG II (10 $\mu g \cdot kg^{-1} \cdot h^{-1}$), respectively. The amplitude of the HR variation during sympathetic stimulation was unchanged by the addition of ANG II. *B*: representative recordings of CSNA under prestimulation baseline and poststimulation conditions. ANG II did not affect the CSNA significantly.

As shown in Table 4, ANG II slightly attenuated the dynamic gain of the sympathetic transfer function to 92.5 ± 8.9% of the value observed under control conditions. ANG II did not affect the natural frequency, damping ratio, or pure delay. The goodness of fit to the second-order low-pass filter did not differ between the control and ANG II conditions. In the HR step response, ANG II did not affect the steady-state response or the 80% rise time. As shown in Table 5, there were no significant differences in the parameters of the sympathetic transfer function between repeated estimations with an intervening interval of more than 20 min.

Table 3. *Mean values for HR, AP, and CSNA obtained using the sympathetic stimulation protocol*

	Control	ANG II	*P* Value
HR, beats/min			
Prestimulation	267±16	261±19	0.21
During stimulation	317±26	311±23	0.063
Difference†	50±21	50±21	0.94
AP, mmHg			
Prestimulation	74±6	106±15*	0.0011
During stimulation	78±6	110±17*	0.0023
Difference†	4.7±3.6	4.1±5.4	0.71
CSNA, μV			
Prestimulation	0.91±0.71 (100%)	0.98±0.78 (99±19%)	0.22
Poststimulation	0.93±0.72 (101±4%)	1.02±0.81 (104±21%)	0.18

Data are means ± SD values; $n = 7$ except for CSNA data where $n = 5$. †The difference was calculated by subtracting the prestimulation value from the value obtained during the sympathetic stimulation period in each animal. *$P < 0.01$ based on a paired *t*-test. Exact *P* values are also shown.

DISCUSSION

Intravenous administration of ANG II at 10 $\mu g \cdot kg^{-1} \cdot h^{-1}$ increased AP but did not affect mean HR or mean CSNA during prestimulation baseline conditions (Tables 1 and 3), suggesting that ANG II at this dose did not affect the residual sympathetic tone to the heart significantly. ANG II significantly attenuated the dynamic gain of the transfer function from vagal stimulation to HR, whereas it only slightly attenuated that of the transfer function from sympathetic stimulation to HR (Tables 2 and 4).

Effects of ANG II on the transfer function from vagal stimulation to HR. ANG II attenuated the dynamic gain of the transfer function from vagal stimulation to HR without affecting the corner frequency or pure delay (Fig. 2 and Table 2). Several interventions can affect the dynamic gain of the vagal transfer function and significantly change the corner frequency. For example, inhibition of cholinesterase, which interferes with the rapid hydrolysis of ACh, augments the dynamic gain and decreases the corner frequency (29). Moreover, blockade of muscarinic K^+ channels, which interferes with fast, membrane-delimited signal transduction, has been shown to attenuate the dynamic gain and decrease the corner frequency (26).

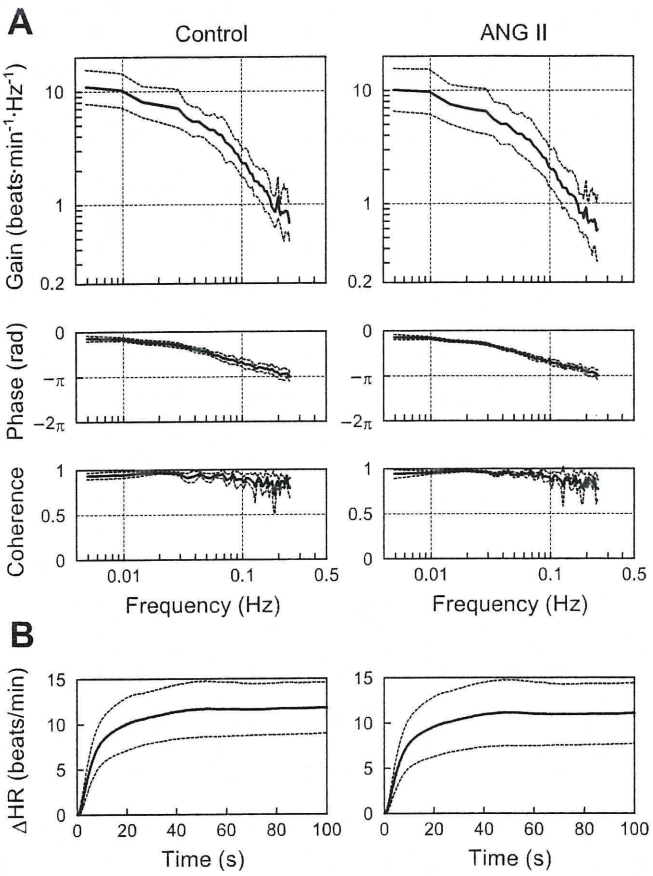

Fig. 4. *A*: averaged transfer functions from cardiac sympathetic nerve stimulation to the HR response obtained before and during intravenous administration of ANG II. Gain plots (*top*), phase plots (*middle*), and coherence plots (*bottom*) are shown. *B*: step responses of the HR to a unit change in the sympathetic stimulation calculated using the transfer functions. ΔHR, changes in heart rate. Solid lines indicate mean, and dashed lines indicate mean ± SD.

On the other hand, several other interventions have been shown to alter the dynamic gain of the vagal transfer function without changing the corner frequency. Concomitant cardiac sympathetic nerve stimulation or increased intracellular cyclic AMP levels augments the dynamic gain without affecting the corner frequency (14, 27), whereas β-adrenergic blockade or high plasma NE attenuates the dynamic gain without affecting the corner frequency (24, 25). Because α-adrenergic blockade nullifies its effects, high plasma NE probably functions via

Table 4. *Effects of intravenous ANG II administration on the parameters of the transfer function and the step response relating to the dynamic sympathetic control of HR*

	Control	ANG II	*P* Value
Dynamic gain, beats·min^{-1}·Hz^{-1}	10.8±2.6	10.2±3.1*	0.049
Natural frequency, Hz	0.069±0.009	0.065±0.006	0.090
Damping ratio	1.53±0.25	1.48±0.21	0.26
Pure delay, s	0.51±0.31	0.42±0.18	0.20
Goodness of fit, %	97.0±1.6	96.9±1.7	0.67
Steady-state response, beats/min	11.8±2.8	11.1±3.4	0.052
80% Rise time, s	17.2±4.7	16.8±4.5	0.62

Data are means ± SD; $n = 7$. *$P < 0.05$ based on a paired *t*-test. Exact *P* values are also shown.

Table 5. *Time effects on the parameters of the transfer function and the step response relating to the dynamic sympathetic control of HR*

	Control 1	Control 2	*P* Value
Dynamic gain, beats·min^{-1}·Hz^{-1}	9.1±1.7	8.6±2.4	0.37
Natural frequency, Hz	0.062±0.014	0.065±0.017	0.10
Damping ratio	1.36±0.22	1.34±0.28	0.75
Pure delay, s	0.65±0.32	0.56±0.25	0.12
Goodness of fit, %	95.8±4.0	97.3±2.2	0.32
Steady-state response, beats/min	9.8±2.0	9.5±2.8	0.55
80% Rise time, s	15.7±3.4	14.4±3.8	0.37

Data are means ± SD; $n = 7$. Exact *P* values are shown.

α-adrenergic receptors on preganglionic and/or postganglionic vagal nerve terminals to limit ACh release during vagal stimulation (24). Our observation that ANG II attenuated the dynamic gain without affecting the corner frequency or pure delay is similar to the results observed with high plasma NE, suggesting that ANG II limits ACh release during vagal stimulation. Although estimated values of the corner frequency ranged from 0.1 to 0.4 among studies, the difference may be attributable to the difference in the input signal properties (see Appendix B for details).

Although Andrews et al. (2) reported that ANG II (500 ng/kg, iv bolus) did not inhibit vagally induced bradycardia in anesthetized ferrets, Potter (31) demonstrated that ANG II (5–10 μg, iv bolus; body weight not shown) attenuated vagally induced bradycardia in anesthetized dogs. The latter study also showed that the addition of ANG II (2–5 μg/25 ml) to an organ bath attenuated vagally induced bradycardia in isolated guinea-pig atria. In that study, ANG II did not attenuate ACh-induced bradycardia, suggesting that the inhibition of bradycardia by ANG II was due to an inhibition of ACh release from vagal nerve terminals (31). In a previous study, we confirmed that intravenous ANG II (10 μg·kg^{-1}·h^{-1}) attenuated myocardial interstitial ACh release in response to vagal nerve stimulation in anesthetized cats (17). The site of this inhibitory action was thought to be parasympathetic ganglia rather than postganglionic vagal nerve terminals, because losartan, an antagonist of the ANG II receptor subtype 1 (AT_1 receptor), abolished the inhibitory action of ANG II when it was administered intravenously but not when it was administered locally through a dialysis fiber. ANG II may also function at the coronary endothelium and produce a diverse range of paracrine effects (6). Although the exact mechanisms remain to be elucidated, intravenous ANG II inhibits ACh release and thereby attenuates the dynamic gain of the vagal transfer function without affecting the corner frequency or pure delay.

Although the observed attenuation of the dynamic HR response to vagal stimulation by ANG II is relatively small, it may have pathophysiological significance as follows. In a previous study, our laboratory has shown that chronic intermittent vagal stimulation significantly improved the survival of chronic heart failure rats after myocardial infarction (21). In that study, the vagal stimulation intensity was such that it reduced HR only by 20 to 30 beats/min (5–10%) in rats. Therefore, change in the vagal effects on the heart, even if relatively small, could affect the evolution of heart failure. Increased plasma or tissue levels of ANG II in heart failure

might attenuate vagal neurotransmission, contributing to the aggravation of disease states.

Effects of ANG II on the transfer function from sympathetic stimulation to HR. Although ANG II attenuated the dynamic gain of the transfer function from sympathetic stimulation to HR without affecting the natural frequency, damping ratio, or pure delay, the attenuating effect was not definitive because the effect was not significant on the steady-state response in the calculated step response (Fig. 4 and Table 4). There are conflicting reports about the effects of ANG II on sympathetic control of the heart. Starke (33) reported that ANG II (1 ng/ml) potentiated NE release in response to postganglionic sympathetic nerve stimulation in isolated rabbit hearts, whereas no effect on spontaneous or tyramine-induced NE output was observed. Farrell et al. (10) demonstrated that administration of ANG II (100 μM at 1 ml/min for 10 min; ~35–42 $\mu g \cdot kg^{-1}$) into right atrial ganglionated plexus neurons via a branch of the right coronary artery caused the release of catecholamine into the myocardial interstitial fluid of anesthetized dogs, suggesting that ANG II affects intrinsic cardiac neurons. In that study, the effect of ANG II on the catecholamine release induced by cardiac sympathetic nerve stimulation was not investigated. On the other hand, Lameris et al. (19) demonstrated that administration of ANG II (0.5 $ng \cdot kg^{-1} \cdot min^{-1}$ or 30 $ng \cdot kg^{-1} \cdot h^{-1}$) into the left anterior descending coronary artery of anesthetized pigs did not yield spontaneous NE release or enhance the NE release induced by cardiac sympathetic nerve stimulation. Cardiac ganglia derived from different species can demonstrate differences in phenotype for ANG II receptors, and this may impact on the resultant neurohumoral interactions. Dendorfer et al. (7) demonstrated that ANG II (0.3 to 1 μg/kg bolus) increased renal sympathetic nerve activity during ganglionic blockade in pithed rats, suggesting direct ganglionic excitation by ANG II. In the present study, because we stimulated the postganglionic cardiac sympathetic nerve, possible direct ganglionic excitation by ANG II might not have affected the dynamic sympathetic control of HR. In addition, postganglionic CSNA did not change significantly in our experimental conditions (Tables 1 and 3), indicating that the 10 $\mu g \cdot kg^{-1} \cdot h^{-1}$ dose of intravenous ANG II was not high enough to produce direct ganglionic excitation.

In isolated rabbit hearts, Peach et al. (30) demonstrated that ANG II (0.2 ng/ml) inhibited NE uptake. Starke (33) reported a higher dose of ANG II (10 μg/ml) to inhibit NE uptake. In a previous study from our laboratory, blockade of neuronal NE uptake using desipramine attenuated the dynamic gain, decreased the natural frequency, and increased the pure delay of the transfer function from sympathetic stimulation to HR (28). In the present study, however, neither the natural frequency nor the pure delay was changed by ANG II, suggesting that NE uptake was not inhibited. In an in vivo study using canine hearts, Lokhandwala et al. (22) demonstrated that ANG II (100 and 200 $ng \cdot kg^{-1} \cdot min^{-1}$ or 6 and 12 $\mu g \cdot kg^{-1} \cdot min^{-1}$ iv) did not affect the positive chronotropic effects of either postganglionic cardiac sympathetic nerve stimulation or intravenous NE infusion. In that study, ANG II enhanced the positive chronotropic effects of sympathetic nerve stimulation but not of intravenous NE infusion after blocking neuronal NE uptake with desipramine. The authors' interpretation of the results was that ANG II facilitated NE release in response to sympathetic nerve stimulation, whereas any effects of ANG II might be masked in animals with functioning neuronal NE uptake mechanisms (22). To make matters more complex, Lameris et al. (19) did not observe enhanced NE release during cardiac sympathetic stimulation in porcine hearts even after neuronal NE uptake was blocked with desipramine. Thus it appears that differences in species, ANG II doses, and experimental settings (in vivo vs. isolated hearts, intravenous vs. intracoronary administration, with or without the contribution of sympathetic ganglia) critically affected the experimental results. Therefore, we believe that assessing the relative effects of ANG II on the vagal and sympathetic systems is important to understand the pathophysiological roles of ANG II in the autonomic regulation of HR.

Limitations. Our results should be interpreted in the context of various experimental limitations. First, we obtained data from anesthetized animals. If the data had been obtained under conscious conditions, the results might have been different. Because we disabled the arterial baroreflexes and cut the autonomic efferent pathways, however, the anesthetics should not have markedly affected our results. Second, because we stimulated the postganglionic cardiac sympathetic nerve, the possible effects of ANG II on the sympathetic ganglia were not assessed. Further studies that stimulate the preganglionic cardiac sympathetic nerve with various doses of ANG II are required to determine the effects of ANG II on the cardiac sympathetic ganglionic transmission. Finally, ANG II may affect the autonomic regulation of HR chronically. Further studies focused on the effects of chronically elevated ANG II levels on the autonomic regulation of HR are required to elucidate the pathophysiological significance of elevated ANG II levels.

In conclusion, continuous intravenous administration of ANG II at a dose that did not induce direct cardiac sympathetic ganglionic excitation significantly attenuated the dynamic gain of the transfer function from vagal stimulation to HR. The attenuation of the transfer gain was observed uniformly in the frequency range under study, suggesting that ANG II can attenuate the HF component of HRV even when vagal outflow from the central nervous system remains unchanged. In addition, the same dose of ANG II did not markedly affect the dynamic gain of the transfer function from postganglionic sympathetic stimulation to HR. Although there remains a room for arguments relating to the different site of stimulation (preganglionic for vagal vs. postganglionic for sympathetic), possible disproportional suppression of the dynamic vagal and sympathetic regulation of HR likely results in a relative dominance of sympathetic control in the presence of ANG II. Because many neurohumoral elements remodel or adapt during the evolution of cardiac pathology (18), we cannot directly extrapolate the results of acute neurohumoral interactions observed in the present study to the chronic pathological situations. If we do so, however, the reduction of the HF component of HRV in patients with cardiovascular diseases, such as myocardial infarction and heart failure (34), may be partly explained by the peripheral effects of ANG II on the dynamic autonomic regulation of HR.

APPENDIX A

Meaning of a step response calculated from a transfer function. We calculated a step response from a transfer function relating to the vagal or sympathetic HR control. The calculated step response is useful for time-domain interpretation of the low-pass filter characteristics described by the frequency-domain transfer function but does not necessarily conform to an experimentally estimated step response because of the following reasons. The transfer function identifies the

linear input-output relationship of a given system around a mean input signal (5 Hz for vagal and 2.5 Hz for sympathetic stimulation in the present study). The step response is then calculated for a unit change in the input signal. If we perform a kind of experiment where we change the stimulation frequency from 4.5 to 5.5 Hz for the vagal system and from 2 to 3 Hz for the sympathetic system, the resultant step response is most likely close to the calculated step response. The ordinary experimental step response is, however, estimated by a step input in which the stimulation is completely turned off before the stimulation starts. The calculated step response and the ordinary experimental step response can conform only when the system is purely linear. Whenever nonlinearities exist such as threshold and saturation commonly observed in biological systems, the two step responses disagree. Conversely, information gained by the ordinary experimental step response has a limited ability to estimate the dynamic HR response unless the system is purely linear.

Once vagal or sympathetic transfer function is identified, an impulse response of the system is obtained by an inverse Fourier transform of the transfer function. We can estimate the dynamic HR response from a convolution of a input signal and the impulse response. Figure 5 represents typical data of measured HR and calculated HR based on the transfer function. Figure 5*A* is a continuation of the time series obtained under the control condition depicted in Fig. 1*A*. Figure 5*B* shows a scatter plot of measured HR versus calculated HR during dynamic vagal stimulation. The solid line indicates a linear regression line ($r^2 = 0.94$). Figure 5*C* is a continuation of the time series obtained under the control condition depicted in Fig. 3*A*. Figure 5*D* shows the scatter plot of measured HR versus calculated HR during dynamic sympathetic stimulation. The solid line indicates a linear regression line. Although a slight convex nonlinearity is noted between the measured HR and calculated HR, squared correlation coefficient is high ($r^2 = 0.89$). These results indicate that the transfer function can represent the dynamic HR response reasonably well.

APPENDIX B

Binary white noise versus Gaussian white noise. In a previous study from our laboratory (29), we reported a corner frequency of ~0.1 Hz for a transfer function from vagal stimulation to HR, which was distinctly different from the result of the present study. Possible explanation for the discrepancy is the difference in the input variance (or power) of vagal stimulation. In the previous study, we used a Gaussian white noise (GWN) with a mean stimulation frequency of 5 Hz and a SD of 2 Hz so that the input signal covered at most 98.8% (means ± 2.5 SD) of the Gaussian distribution when the actual stimulation frequency was limited between 0 and 10 Hz. The variance of the GWN signal is 4 Hz^2. In contrast, the 0–10 Hz binary white noise used in the present study has a variance of 25 Hz^2. Hence, the binary white noise has a merit of increasing the input variance over the GWN when the stimulation frequency is limited between 0 and 10 Hz. Increasing the

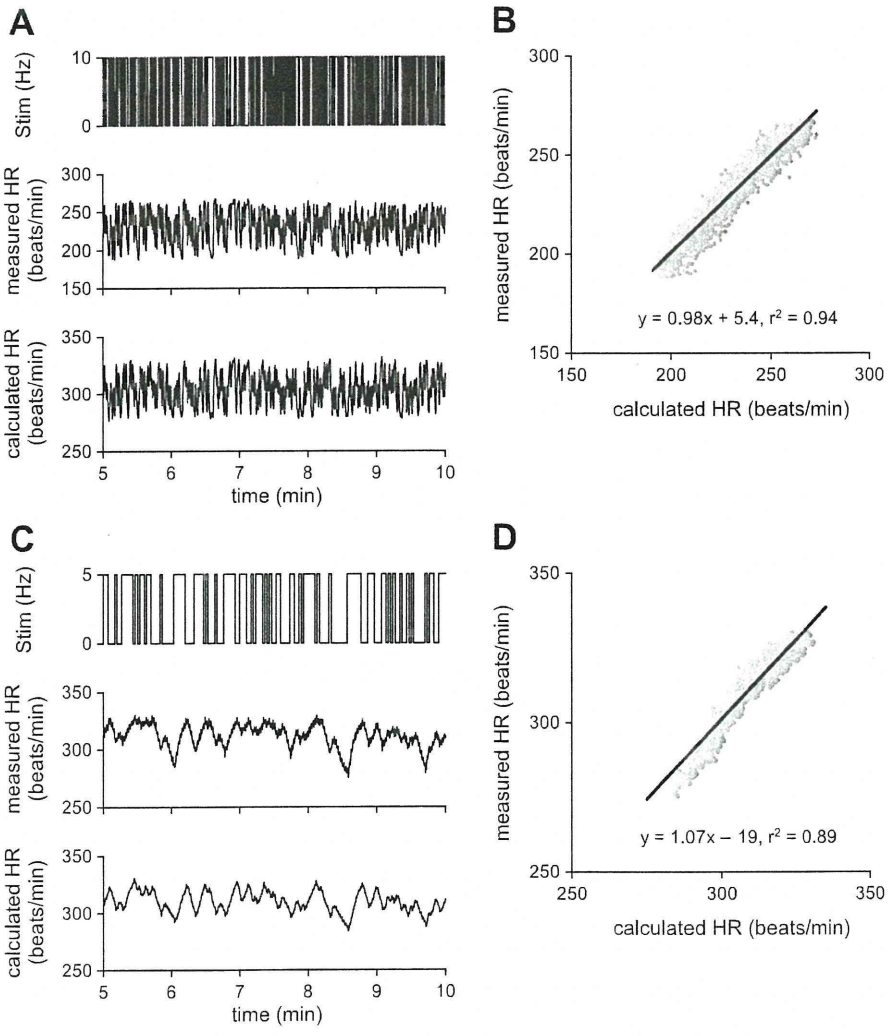

Fig. 5. *A*: data showing vagal stimulation (Stim), measured HR, and calculated HR based on the identified vagal transfer function of this animal. Time axis indicates the minutes after the initiation of random vagal stimulation (continuation of Fig. 1*A*). *B*: scatter plot between measured and calculated HR values. A solid line indicates a liner regression line. *C*: data showing sympathetic stimulation (Stim), measured HR, and calculated HR based on the identified sympathetic transfer function of this animal. Time axis indicates the minutes after the initiation of random sympathetic stimulation (continuation of Fig. 3*A*). *D*: scatter plot between measured and calculated HR values. A solid line indicates a linear regression line.

input variance is effective to increase the signal-to-noise ratio in the output signal and to improve the estimation of the transfer function.

In an earlier study on the transfer function analysis, Berger et al. (3) demonstrated that the roll-off of the vagal transfer function was gentle (i.e., the corner frequency was high) at high mean stimulatory rates and became more abrupt (i.e., the corner frequency was lower) with lower mean stimulatory rates. Although they attributed the difference in the roll-off characteristics to the difference in mean stimulatory rates, because they set the variance of input signal at ~1/4 of the mean stimulatory rates, which of the mean stimulatory rates or the input variance contributed to the determination of corner frequency seems inconclusive. Because there was no significant difference in the corner frequency between the vagal transfer functions estimated by GWNs of 5 ± 2 Hz and 10 ± 2 Hz (means ± SD) in a previous study from our laboratory (29), we speculate that the difference in the input variance rather than the mean stimulation frequency might have caused the different values of the corner frequency between the previous and the present results. This speculation requires further verification in future.

GRANTS

This study was supported by a Health and Labour Sciences Research Grant for Research on Advanced Medical Technology; a Health and Labour Sciences Research Grant for Research on Medical Devices for Analyzing, Supporting, and Substituting the Function of the Human Body; Health and Labour Sciences Research Grants H18-Iryo-Ippan-023, H18-Nano-Ippan-003, and H19-Nano-Ippan-009 from the Ministry of Health, Labour and Welfare of Japan; and the Industrial Technology Research Grant Program from the New Energy and Industrial Technology Development Organization of Japan.

REFERENCES

1. **Akselrod S, Gordon D, Ubel FA, Shannon DC, Berger AC, Cohen RJ.** Power spectrum analysis of heart rate fluctuation: a quantitative probe of beat-to-beat cardiovascular control. *Science* 213: 220–222, 1981.
2. **Andrews PL, Dutia MB, Harris PJ.** Angiotensin II does not inhibit vagally-induced bradycardia or gastric contractions in the anaesthetized ferret. *Br J Pharmacol* 82: 833–837, 1984.
3. **Berger RD, Saul JP, Cohen RJ.** Transfer function analysis of autonomic regulation. I. Canine atrial rate response. *Am J Physiol Heart Circ Physiol* 256: H142–H152, 1989.
4. **Brigham EO.** FFT transform applications. In: *The Fast Fourier Transform and Its Applications*. Englewood Cliffs, NJ: Prentice-Hall, 1988, p. 167–203.
5. **Brooks VL.** Chronic infusion of angiotensin II resets baroreflex control of heart rate by an arterial pressure-independent mechanism. *Hypertension* 26: 420–424, 1995.
6. **Castillo-Hernandez JR, Rubio-Gayosso I, Sada-Ovalle I, Garcia-Vazquez A, Ceballos G, Rubio R.** Intracoronary angiotensin II causes inotropic and vascular effects via different paracrine mechanisms. *Vascul Pharmacol* 41: 147–158, 2004.
7. **Dendorfer A, Thornagel A, Raasch W, Grisk O, Tempel K, Dominiak P.** Angiotensin II induces catecholamine release by direct ganglionic excitation. *Hypertension* 40: 348–354, 2002.
8. **DiBona GF.** Physiology in perspective: the wisdom of the body. Neural control of the kidney. *Am J Physiol Regul Integr Comp Physiol* 289: R633–R641, 2005.
9. **Diz DI, Averill DB.** Angiotensin II/autonomic interactions. In: *Primer on the Autonomic Nervous System*, edited by Robertson D, Biaggioni I, Burnstock G, and Low PA. San Diego: Elsevier Academic Press, 2004, p. 168–171.
10. **Farrell DM, Wei CC, Tallaj J, Ardell JL, Armour JA, Hageman GR, Bradley WE, Dell'Italia LJ.** Angiotensin II modulates catecholamine release into interstitial fluid of canine myocardium in vivo. *Am J Physiol Heart Circ Physiol* 281: H813–H822, 2001.
11. **Glantz SA.** *Primer of Biostatistics* (5th ed.). New York: McGraw-Hill, 2002.
12. **Jackson EK.** Autonomic control of the kidney. In: *Primer on the Autonomic Nervous System*, edited by Robertson D, Biaggioni I, Burnstock G, and Low PA. San Diego: Elsevier Academic Press, 2004, p. 157–161.
13. **Kashihara K, Takahashi Y, Chatani K, Kawada T, Zheng C, Li M, Sugimachi M, Sunagawa K.** Intravenous angiotensin II does not affect dynamic baroreflex characteristics of the neural or peripheral arc. *Jpn J Physiol* 53: 135–143, 2003.
14. **Kawada T, Ikeda Y, Sugimachi M, Shishido T, Kawaguchi O, Yamazaki T, Alexander J Jr, Sunagawa K.** Bidirectional augmentation of heart rate regulation by autonomic nervous system in rabbits. *Am J Physiol Heart Circ Physiol* 271: H288–H295, 1996.
15. **Kawada T, Miyamoto T, Miyoshi Y, Yamaguchi S, Tanabe Y, Kamiya A, Shishido T, Sugimachi M.** Sympathetic neural regulation of heart rate is robust against high plasma catecholamine. *J Physiol Sci* 56: 235–245, 2006.
16. **Kawada T, Uemura K, Kashihara K, Jin Y, Li M, Zheng C, Sugimachi M, Sunagawa K.** Uniformity in dynamic baroreflex regulation of left and right cardiac sympathetic nerve activities. *Am J Physiol Regul Integr Comp Physiol* 284: R1506–R1512, 2003.
17. **Kawada T, Yamazaki T, Akiyama T, Li M, Zheng C, Shishido T, Mori H, Sugimachi M.** Angiotensin II attenuates myocardial interstitial acetylcholine release in response to vagal stimulation. *Am J Physiol Heart Circ Physiol* 293: H2516–H2522, 2007.
18. **Khan MH, Sinoway LI.** Congestive heart failure. In: *Primer on the Autonomic Nervous System*, edited by Robertson D, Biaggioni I, Burnstock G, and Low PA. San Diego: Elsevier Academic Press, 2004, p. 247–248.
19. **Lameris TW, de Zeeuw S, Duncker DJ, Alberts G, Boomsma F, Verdouw PD, van den Meiracker AH.** Exogenous angiotensin II does not facilitate norepinephrine release in the heart. *Hypertension* 40: 491–497, 2002.
20. **Levy MN.** Sympathetic-parasympathetic interactions in the heart. *Circ Res* 29: 437–445, 1971.
21. **Li M, Zheng C, Sato T, Kawada T, Sugimachi M, Sunagawa K.** Vagal nerve stimulation markedly improves long-term survival after chronic heart failure in rats. *Circulation* 109: 120–124, 2004.
22. **Lokhandwala MF, Amelang E, Buckley JP.** Facilitation of cardiac sympathetic function by angiotensin II: role of presynaptic angiotensin receptors. *Eur J Pharmacol* 52: 405–409, 1978.
23. **Marmarelis PZ, Marmarelis VZ.** The white noise method in system identification. In: *Analysis of Physiological Systems*. New York: Plenum, 1978, p. 131–221.
24. **Miyamoto T, Kawada T, Takaki H, Inagaki M, Yanagiya Y, Jin Y, Sugimachi M, Sunagawa K.** High plasma norepinephrine attenuates the dynamic heart rate response to vagal stimulation. *Am J Physiol Heart Circ Physiol* 284: H2412–H2418, 2003.
25. **Miyamoto T, Kawada T, Yanagiya Y, Inagaki M, Takaki H, Sugimachi M, Sunagawa K.** Cardiac sympathetic nerve stimulation does not attenuate dynamic vagal control of heart rate via α-adrenergic mechanism. *Am J Physiol Heart Circ Physiol* 287: H860–H865, 2004.
26. **Mizuno M, Kamiya A, Kawada T, Miyamoto T, Shimizu S, Sugimachi M.** Muscarinic potassium channels augment dynamic and static heart rate responses to vagal stimulation. *Am J Physiol Heart Circ Physiol* 293: H1564–H1570, 2007.
27. **Nakahara T, Kawada T, Sugimachi M, Miyano H, Sato T, Shishido T, Yoshimura R, Miyashita H, Inagaki M, Alexander J Jr, Sunagawa K.** Accumulation of cAMP augments dynamic vagal control of heart rate. *Am J Physiol Heart Circ Physiol* 275: H562–H567, 1998.
28. **Nakahara T, Kawada T, Sugimachi M, Miyano H, Sato T, Shishido T, Yoshimura R, Miyashita H, Inagaki M, Alexander J Jr, Sunagawa K.** Neuronal uptake affects dynamic characteristics of heart rate response to sympathetic stimulation. *Am J Physiol Regul Integr Comp Physiol* 277: R140–R146, 1999.
29. **Nakahara T, Kawada T, Sugimachi M, Miyano H, Sato T, Shishido T, Yoshimura R, Miyashita H, Sunagawa K.** Cholinesterase affects dynamic transduction properties from vagal stimulation to heart rate. *Am J Physiol Regul Integr Comp Physiol* 275: R541–R547, 1998.
30. **Peach MJ, Bumpus FM, Khairallah PA.** Inhibition of norepinephrine uptake in hearts by angiotensin II and analogs. *J Pharmacol Exp Ther* 167: 291–299, 1969.
31. **Potter EK.** Angiotensin inhibits action of vagus nerve at the heart. *Br J Pharmacol* 75: 9–11, 1982.
32. **Reid IA, Chou L.** Analysis of the action of angiotensin II on the baroreflex control of heart rate in conscious rabbits. *Endocrinology* 126: 2749–2756, 1990.
33. **Starke K.** Action of angiotensin on uptake, release and metabolism of ^{14}C-noradrenaline by isolated rabbit hearts. *Eur J Pharmacol* 14: 112–123, 1971.
34. **Task Force of the European Society of Cardiology, the North American Society of Pacing and Electrophysiology.** Heart rate variability: standards of measurement, physiological interpretation and clinical use. *Circulation* 93: 1043–1065, 1996.
35. **Zimmerman BG, Sybertz EJ, Wong PC.** Interaction between sympathetic and renin-angiotensin system. *J Hypertens* 2: 581–587, 1984.